TIPE drives a cancer stem-like phenotype by promoting glycolysis via PKM2/HIF-1α axis in melanoma

Maojin Tian[1#], Le Yang[2#], Ziqian Zhao[3#], Jigang Li[1], Lianqing Wang[1], Qingqing Yin[2], Wei Hu[1], Yunwei Lou[4], Jianxin Du[1*], Peiqing Zhao[1*]

[1] *Center of Translational Medicine, Zibo Central Hospital Affiliated to Binzhou Medical University, Zibo, 255036, PR China*

[2] *Shandong First Medical University, Jinan,250117, PR China*

[3] *The Second Medical College, Xinjiang Medical University, Urumqi, 830092, PR China*

[4] *School of Laboratory Medicine, Xinxiang Medical University, Xinxiang,453003, PR China*

[#] Contributed equally

* Correspondence to: Peiqing Zhao, Center of Translational Medicine, Zibo Central Hospital Affiliated to Binzhou Medical University, Zibo, China, 54 Gongqingtuan Xi Road, Zibo 255036, PR China. Jianxin Du, Center of Translational Medicine, Zibo Central Hospital Affiliated to Binzhou Medical University, Zibo, China, 54 Gongqingtuan Xi Road, Zibo 255036.

Tel: +86 533 2365217 Fax: +86 533 2360819

E-mail: bzjzzpq@sdu.edu.cn or bzjzzpq@163.com (Peiqing Zhao); jianxindu2005@126.com (Jianxin Du)

Abstract

TIPE (TNFAIP8) has been identified as an oncogene and participates in tumor biology. However, how its role in the metabolism of tumor cells during melanoma development remains unclear. Here, we demonstrated that TIPE promoted glycolysis by interacting with pyruvate kinase M2 (PKM2) in melanoma. We found that TIPE induced PKM2 dimerization, thereby facilitating its translocation from the cytoplasm to the nucleus. TIPE-mediated PKM2 dimerization consequently promoted HIF-1α activation and glycolysis, which contributed to melanoma progression and increased its stemness features. Notably, TIPE specifically phosphorylated PKM2 at Ser 37 in an ERK-dependent manner. Consistently, the expression of TIPE was positively correlated with the levels of PKM2 Ser37 phosphorylation and cancer stem cell markers in melanoma tissues from clinical samples and tumor bearing mice. In summary, our findings indicate that the TIPE/PKM2/HIF-1α signaling pathway plays a pivotal role in promoting cancer stem cell properties by facilitating the glycolysis, which would provide a promising therapeutic target for melanoma intervention.

Keywords: TIPE, Glycolysis, PKM2, HIF-1α, Melanoma

Introduction

Melanoma is derived from the aberrant growth of melanocytes and is classified into several subgroups such as cutaneous melanoma (CM), uveal melanoma (UM), and mucosal melanoma (MM), based on its tissue locations(Han et al., 2021). Cutaneous melanoma (CM) is the major subgroup of melanoma. Accumulating evidence has revealed that metabolic reprogramming contributes to the tumorigenesis and progression of melanoma. Owing to its low incidence rate, targeting metabolism might be a promising therapeutic approach for the treatment of melanoma and offers a deeper understanding of its pathobiology(Brunner and Finley, 2022; Faubert et al., 2020). However, melanoma-altered metabolic reprogramming remains poorly understood.

The Warburg effect, also known as aerobic glycolysis, is a part of metabolic reprogramming. It increases lactate levels regardless of oxygen availability in tumor cells, providing cancer cell tumorigenicity, progression, and chemoresistance(Guo et al., 2022). Pyruvate kinase isoform M2 (PKM2) is the key enzyme that irreversibly converts phosphoenolpyruvate (PEP) to pyruvate in the last step of glycolysis (Li et al., 2016; Liu et al., 2021). It is shifted between catalytically inactive

74 dimeric and active tetrameric forms, and the PKM2 dimer predominantly
75 serves as a key glycolytic enzyme that provides advantages for tumor
76 progression due to the Warburg effect(Liu et al., 2017). Post-translational
77 modifications of PKM2, such as FGFR1-mediated Tyr105
78 phosphorylation and ERK1/2-dependent Ser37 phosphorylation, can
79 promote PKM2 from a tetrameric to dimeric form, accelerating its
80 translocation into the nucleus (Christofk et al., 2008; Li et al., 2016). In
81 the nucleus, PKM2 acts as a protein kinase that phosphorylates
82 STAT3(Chen et al., 2022a; Dhanesha et al., 2022) and Histone H3(Niu et
83 al., 2020). Interestingly, nuclear PKM2 also functions as a coactivator for
84 several transcription factors, such as HIF-1α(Luo et al., 2011; Wang et al.,
85 2014) or Oct4(Yang et al., 2018), by which regulates metabolic gene
86 transcription and promotes tumorigenesis or sustains cancer stem cell
87 populations. Furthermore, HIF-1α is constitutively activated in melanoma
88 under both normal and hypoxic conditions and is accompanied by
89 increased glycolysis(D'Aguanno et al., 2021; Malekan et al., 2021).
90 Therefore, the precise mechanisms underlying PKM2 activity regulation
91 and its function as an HIF-1α coactivator might provide a molecular basis
92 for the melanoma targeted therapy.

93 The tumor necrosis factor alpha-induced protein 8 (TNFAIP8, TIPE)
94 family is composed of four members: TIPE, TIPE1, TIPE2, and
95 TIPE3(Yang et al., 2022). Accumulating evidence suggests that TIPE is

96 strongly associated with the development of various cancers by affecting
97 cell proliferation, apoptosis, invasion, and metastasis(Goldsmith et al.,
98 2017; Niture et al., 2018). Therefore, TIPE is broadly considered pro-
99 cancerous(Padmavathi et al., 2018). However, we previous revealed that
100 TIPE functions as a tumor suppressor in colitis and colitis-associated
101 colon cancer(Lou et al., 2022), indicating that TIPE might serve a
102 multifarious function in malignancies. Hitherto, the role of TIPE in
103 melanoma remains unclear. In this study, we revealed that TIPE-mediated
104 PKM2 Ser37 phosphorylation accelerates PKM2 translocation from the
105 cytoplasm to the nucleus, thereby elevating its binding ability to HIF-1α
106 and hypoxia response elements (HREs), thus promoting metabolic
107 reprogramming. TIPE-mediated metabolic reprogramming can confer
108 tumorigenesis and stem-like phenomena to melanoma cells. This process
109 represents an important regulator of the TIPE family switching between
110 oxidative phosphorylation and aerobic glycolysis, paving the way for
111 cancer-specific metabolism in response to low-oxygen challenge.
112

113 # Results

114 **TIPE increases aerobic glycolysis in melanoma cells**

115 To characterize how TIPE performs biological functions in melanoma, we
116 examined its expression levels in melanoma cell lines. The results
117 showed that A375 and A875 cells had relatively higher TIPE expression

than G361 and MM96L cells. Therefore, we downregulated TIPE expression in A375 cells and overexpressed TIPE in G361 cells to perform further experiments (**Fig.S1**). Furthermore, we demonstrated that TIPE promotes melanoma tumorigenesis both *in vitro* and *in vivo*(**Fig.S2**).

Consequently, we performed RNA sequencing analysis by overexpressing TIPE in G361 cells (**Fig. 1A**) to examine the underlying mechanisms involved in the progression of melanoma. The results revealed that the overexpression of TIPE dramatically promoted glycolysis metabolites and the HIF-1α pathway (**Fig. 1B, C**). Since metabolic reprogramming, especially aerobic glycolysis, is tightly dependent on the HIF-1α pathway(Baik et al., 2019), we assumed that TIPE promotes melanoma progression might via the regulation of metabolic reprogramming. Therefore, we performed a metabolomic analysis after interfering with TIPE in A375 cells. Interestingly, the results indicated that the aerobic glycolysis pathway, including pyruvate and lactate, was significantly inhibited in melanoma cells after TIPE silencing (**Fig. 1D**), confirming that TIPE facilitates glycolytic metabolism in melanoma. Consequently, ATPase activity, lactate secretion, and ATP content assays were performed to further confirm TIPE-induced glycolytic changes. The results demonstrated that TIPE decreased ATPase activity and ATP content while promoting lactate

140 production (**Fig. 1E-G**). Additionally, we measured the extracellular
141 acidification rate (ECAR) after the overexpression or downregulation of
142 TIPE using a Seahorse Bioscience Flux Analyzer. The results also
143 revealed that TIPE promoted glycolysis and glycolytic capacity in
144 melanoma cells (**Fig. 1H-K**).

145 Furthermore, we investigated whether TIPE affected HIF-1α
146 transcriptional activity or its expression levels. The results demonstrated
147 that TIPE increased the expression of HIF-1α at both mRNA and protein
148 levels(**Fig. S3**). Interestingly, TIPE can dramatically activate the hypoxia
149 response element(HRE) reporter activity, with which HIF-1α is more
150 prone to recognize the specific DNA motif to regulate metabolic gene
151 transcription(Chen et al., 2022b)(**Fig. 1L**).

152 Collectively, above results demonstrate that TIPE plays a crucial role in
153 promoting melanoma glycolysis. However, the impact of TIPE on the
154 Warburg effect by regulating HIF-1α activity requires further
155 investigation.

156 **TIPE interacts with PKM2, promotes its dimerization and nuclear**
157 **import**

158 To further study the functions of TIPE in melanoma, we used the Co-
159 IP/MS method to bait the potential binding partners of TIPE (the
160 candidate interacting proteins of TIPE are listed in **Table S1**).
161 Interestingly, we found that PKM2, the key enzyme in aerobic glycolysis,

162 might be a new partner of TIPE in melanoma (**Fig. 2A**) (**Fig. S4**). Next,
163 we performed Co-IP assays to confirm the interactions between TIPE and
164 PKM2. The results revealed that exogenously overexpressed Flag-tagged
165 PKM2 interacted with exogenously overexpressed HA-tagged TIPE (**Fig.**
166 **2B, C**). Furthermore, endogenous interactions between PKM2 and TIPE
167 were confirmed in the A375 cells (**Fig. 2D, E**). GST-pull down assays
168 demonstrated that TIPE directly bound to PKM2 *in vitro* (**Fig. 2F**).
169 Moreover, we performed Doulink assay to further demonstrate their
170 endogenous interactions. The results also showed that endogenous
171 interactions between TIPE and PKM2 were confirmed in G361 cells (**Fig.**
172 **2G**). Based on these interactions, we identified the binding regions
173 between TIPE and PKM2. We generated four fragments of PKM2,
174 including amino acids 1-390(NA1BA2), 45-390(A1BA2), 1-219(NA1B)
175 and 220-390(A2), based on their structural domains (**Fig. 2H**). The
176 results showed that except for the A2 domain, the NA1BA2, A1BA2, and
177 NA1B domains of PKM2 were necessary for its interaction with TIPE
178 (**Fig. 2I**). Finally, the TIPE protein was divided into two fragments,
179 including amino acids 1-100 (M1) and 101-198 (M2). The data showed
180 that the amino acids 1-100(M1) and 101-198(M2) of TIPE interacted with
181 PKM2 (**Fig. 2J**). Taken together, these data revealed that TIPE interacts
182 with PKM2.

183 Since TIPE interacts with PKM2 in melanoma, we determined whether

184 TIPE increases aerobic glycolysis by affecting PKM2 expression or its
185 activity. The results showed that TIPE did not influence the expression of
186 PKM2 at either the mRNA or the protein level (**Fig. S5**). Intriguingly, we
187 demonstrated that dimeric PKM2 was reduced in TIPE-silenced A375
188 cells (**Fig. 2K**) and was increased following TIPE overexpression in
189 G361 cells (**Fig. 2L**). Normally, a dimeric form of PKM2 with low
190 affinity for its substrate, phosphoenolpyruvate (PEP), and a tetrameric
191 form have a high PEP affinity. Moreover, the dimeric form of PKM2 is
192 more prone to translocation into the nucleus and thus exerts protein
193 kinase activity, which confers the Warburg effect and tumorigenesis(Zhou
194 et al., 2022). Western blot analysis of nuclear and cytosolic fractions from
195 A375 cells revealed that PKM2 primarily resided in the cytoplasm in
196 which TIPE was downregulated. Likewise , the nuclear level of PKM2
197 was increased after overexpression of TIPE in G361 cells (**Fig. 2M**).
198 Furthermore, we examined the distribution of PKM2 after TIPE
199 overexpression by using a Thermo Fisher EVOS microscopic analysis. As
200 shown in **Fig.2N**, PKM2 was predominantly present in the nucleus after
201 TIPE overexpression, and this phenomenon was diminished by the
202 administration of a PKM2 dimer formation suppressor (TEPP-46,
203 100μM). It has been shown that dimeric PKM2 promotes tumor
204 progression by regulating the Warburg effect(Zhou et al., 2022). Thus, we
205 speculated that TIPE restores the nuclear levels of PKM2 to promote

206 melanoma tumorigenicity via a dimeric PKM2-dependent Warburg effect.

207 **TIPE requires PKM2 for transcriptional activation of HIF-1α**

208 Accumulating evidence has revealed that tetrameric PKM2 is
209 enzymatically active towards pyruvate and acts as a transcriptional
210 coactivator, while it dissociates into a dimer(Wei et al., 2020).
211 Consequently, the dimeric form of PKM2 becomes a coactivator of HIF-
212 1α to transcriptionally activate glycolytic genes in favor of the Warburg
213 effect (**Fig.3A**)(Ouyang et al., 2018). As PKM2 and HIF-1α both play
214 important roles in the metabolic reprogramming process, it is reasonable
215 to believe that the interactions between TIPE and these two molecules
216 could affect the glycolysis in melanoma. Thus, we investigated whether
217 TIPE promoted the transcriptional activation of HIF-1α in a PKM2-
218 dependent manner.

219 To confirm the effect of TIPE activation on HIF-1α transcriptional
220 activity, we tested the ability of TIPE to activate the HRE reporter
221 activity in HRE-luciferase plasmid transfected HEK-293T cells. Not
222 surprisingly, significant augmentation of HRE promoter activation by
223 TIPE was observed, especially when combined with PKM2 (**Fig.3B**).
224 Consequently, TIPE activated HRE reporter activity in a dose-dependent
225 manner, and this phenomenon was reversed after PKM2 knockdown,
226 demonstrating that TIPE has critical effects on the activation of HIF-1α
227 transcription in a PKM2-dependent manner (**Fig.3C**). HIF-1α targeted

genes such as *LDHA* and *GLUT1* were also upregulated by TIPE in a dose-dependent manner and were reversed by interfering with PKM2 (**Fig.3D, E**). Due to PKM2 cooperated with HIF-1α to activate glycolytic genes during the Warburg effect, we used the Duolink method to confirm whether TIPE affects the endogenous interaction between HIF-1α and PKM2. The results showed that the interaction between HIF-1α and PKM2 was decreased by TIPE interference, whereas the interaction was increased when TIPE was overexpressed (**Fig.3F, G**). More interestingly, TIPE enhanced the PKM2/HIF-1α interaction in the nucleus, further indicating that TIPE induced PKM2 nuclear translocation and thus promoted its interaction with HIF-1α (**Fig.3H**). In addition, the Co-IP assay revealed that TIPE elevated this interaction in a dose-dependent manner (**Fig.3I**).

Moreover, we analyzed the correlation between TIPE and hypoxia scores using TCGA dataset. Interestingly, we found that the hypoxia score was significantly related to the expression of TIPE (**Fig.3J**) (**Table S2**), and the TIPE higher expression group had a higher hypoxia score than the lower expression group in melanoma (**Fig.3K**).

Collectively, these results demonstrated that TIPE has critical effects on the transcriptional activation of HIF-1α in a PKM2-dependent manner.

TIPE promotes HIF-1α transcriptional activation via PKM2 Ser37 phosphorylation

250 The presence of PKM2 in the nucleus enhances glucose metabolism by
251 regulating HIF-1α(Luo et al., 2011). Our results preliminarily
252 demonstrate that TIPE promotes PKM2 dimerization and nuclear import,
253 thereby increasing HIF-1α transcriptional activation and promoting
254 aerobic glycolysis. Normally, Erk1/2-dependent phosphorylation of
255 PKM2 at serine 37 (Ser37) and FGFR1-dependent phosphorylation of
256 PKM2 at tyrosine 105 (Tyr105)(Li et al., 2016; Zhou et al., 2018) are
257 indicative of its dimerization and translocation, further promoting the
258 Warburg effect and serving as a transcription factor
259 coactivator(Novoyatleva et al., 2019; Wei et al., 2020). As shown in
260 **Fig.4A**, interference with TIPE in A375 cells blocked PKM2 Ser37
261 phosphorylation, and overexpression of TIPE in G361 cells caused Ser37
262 phosphorylation compared to controls. However, the phosphorylation of
263 PKM2 Tyr105 did not show any obvious changes. Consequently, we
264 hypothesized that this transformation caused by Ser37 phosphorylation
265 affects the interaction between TIPE and PKM2. As expected, the
266 mutation of PKM2 at S37A blocked its interaction with TIPE, but not
267 with the Y105D mutation (**Fig.4B**). Interestingly, this mutation also
268 interfered with the interaction between PKM2 and HIF-1α, which was
269 elevated by TIPE overexpression (**Fig.4C**). A previous study has revealed
270 that TIPE promotes chemoresistance in acute myeloid leukemia (AML)
271 by activating the ERK signaling pathway(Pang et al., 2020). In addition,

272 phosphorylation of PKM2 at serine 37 is ERK1/2-dependent
273 manner(Yang et al., 2012). TIPE does not serve as a phosphorylase to
274 perform such post-translational modifications directly. Taken together,
275 these results indicate that TIPE promotes PKM2 dimerization depending
276 on ERK signaling. As expected, the ERK inhibitor, U0126, inhibited
277 PKM2 Ser37 phosphorylation induced by TIPE overexpression (**Fig.4D**).
278 To investigate whether TIPE affects the binding affinity of PKM2 to the
279 Hif-1α specific binding site of the *LDHA* and *GLUT1* promoter using
280 chromatin immunoprecipitation *q*PCR (ChIP-*q*PCR) analysis, we found
281 that TIPE increased the binding of PKM2 to the *LDHA* and *GLUT1*
282 promoters. This phenomenon, caused by the overexpression of TIPE, was
283 diminished after the administration of TEPP-46, indicating that TIPE
284 promoted the binding of PKM2 to the *LDHA* and *GLUT1* promoters in a
285 dimeric PKM2-dependent manner (**Fig.4E, F**). Finally, we demonstrated
286 that the augmentation of TIPE on HRE promoter activation or HIF-1α
287 targeted genes such as *LDHA* and *GLUT1* was blocked by the S37A
288 mutation (**Fig.4G-I**).

289 In brief, we revealed that TIPE promoted HIF-1α transcriptional
290 activation via ERK-dependent PKM2 Ser37 phosphorylation.

291 **TIPE facilitates melanoma tumorigenesis and aerobic glycolysis in a**
292 **dimeric PKM2-dependent manner**

293 Several studies have demonstrated that dimeric PKM2 increases tumor

294 progression by regulating the Warburg effect. Therefore, we speculated
295 that TIPE promotes melanoma growth through a dimeric PKM2-
296 dependent Warburg effect. To demonstrate this, we knocked down TIPE
297 in A375 cells and found that cell proliferation was decreased.
298 Interestingly, we found that Pyridoxine, a PKM2 dimer formation inducer
299 (Wei et al., 2020), was sufficient to abrogate the TIPE silencing-mediated
300 cell proliferation (**Fig.5A**). Consistently, TEPP-46, a PKM2 dimer
301 formation suppressor, was sufficient to reverse the increased proliferative
302 capacity induced by TIPE-overexpression in G361 cells (**Fig.5B**). Clone
303 formation ability (**Fig.5C, D**) and *in vivo* experiments (**Fig.5E-G**) also
304 demonstrated this phenomenon. Interestingly, we found that decreased
305 ECAR, glycolysis, and glycolytic capacity induced by TIPE interference
306 could be fully antagonized by Pyridoxine in A375 cells (**Fig.5H-J**). In
307 addition, TEPP-46 reversed the ECAR, glycolysis, and glycolytic
308 capacity induced by TIPE overexpression in G361 cells (**Fig.5K-M**).
309 Lastly, to further demonstrate how TIPE affects the PKM2/HIF-1α
310 pathway during the Warburg effect, we revealed that inhibition of PKM2
311 dimerization can rescue TIPE-induced cell proliferation. However, this
312 phenomenon was diminished by the activation of HIF-1α, demonstrating
313 that TIPE promotes melanoma cell proliferation via dimeric PKM2
314 dependent HIF-1α activation (**Fig.5N, O**). More interestingly, we
315 evidenced that suppression of PKM2 dimerization inhibited the TIPE-

316 mediated Warburg effect. In addition, this phenomenon was diminished
317 by the activation of HIF-1α (**Fig.5P, Q**).

318 Taken together, these data suggest that TIPE regulates cell growth and
319 the Warburg effect by inducing the formation of dimeric PKM2, and thus
320 activating the HIF-1α pathway.

321 **TIPE accelerates melanoma cells stem-like phenomenon via**
322 **promoting PKM2 dimerization under normoxic conditions**

323 Increasing evidence has shown that the HIF-1α pathway is associated
324 with acquisition of cancer stem-like properties(Weinstein et al., 2022;
325 Zhu et al., 2022). To confirm the effects of TIPE on the stemness of
326 melanoma cells under normoxic conditions, we examined the stemness-
327 associated features *in vitro*. First, we measured cancer stem-like
328 phenotype markers, including *NANOG*, *NOTCH*, *OCT3/4*, *SOX2* and
329 *BMI-1*. The results showed that the markers were increased after
330 overexpression of TIPE in G361 cells (**Fig.6A**) and were reduced after
331 TIPE interference in A375 cells by using *q*PCR method (**Fig.6B**). We
332 further revealed that TIPE increased the migration ability and increased
333 sphere formation (**Fig.6C, D**). In addition, TIPE significantly increased
334 the chemosensitivity of melanoma cell to sorafenib (**Fig.6E, F**). Next, we
335 examined the tumorigenicity of melanoma cells with TIPE knockdown *in*
336 *vivo* by injecting Ctrl-sh or TIPE-sh A375 cells subcutaneously into nude
337 mice at three dilutions (1×10^6, 1×10^5 and 1×10^4) and allowing them to

338 grow for four weeks. The Confidence intervals (CIs) for 1/ (stem cell
339 frequency) using extreme limiting dilution were calculated as previous
340 reported(Hu and Smyth, 2009; Niu et al., 2021). The estimated CI for the
341 frequency of CSCs in the TIPE knockdown group was 202749, compared
342 with 18441 in the control group (P<0.001) (**Fig.6G**) (**Table S3, 4**).
343 Moreover, $CD44^+$ subpopulations were significantly elevated, as detected
344 using a fluorescence-activated cell sorting (FACS) assay (**Fig.6H, I**).
345 Because TIPE promotes HIF-1α transcriptional activation in a dimeric
346 PKM2-dependent manner, we performed a sphere formation assay by
347 overexpressing TIPE in G361 cells. The results showed that TEPP-46
348 partially reversed mammosphere formation induced by TIPE
349 overexpression. Moreover, overexpression of HIF-1α diminished this
350 phenomenon, indicating that TIPE-induced sphere formation depended on
351 dimeric PKM2-dependent HIF-1α activation (**Fig.6J**). In addition, the
352 increased $CD44^+$ subpopulations of G361 cells induced by TIPE were
353 decreased by the administration of TEPP-46, and could be rescued by
354 overexpression of HIF-1α(**Fig.6K**).
355 These findings strongly suggest that TIPE maintains melanoma cell
356 stemness via dimeric PKM2-dependent HIF-1α activation.
357 **TIPE is positively correlated with the levels of PKM2 Ser37**
358 **phosphorylation and cancer stem cell markers**
359 We analyzed the expression of TIPE in melanoma and benign skin

360 tumors, and the results showed that the expression of TIPE was
361 dramatically increased compared to controls using a tissue chip (**Fig.7A,**
362 **B**). To determine if there was a correlation between TIPE and PKM2
363 Ser37 levels, TIPE and PKM2 Ser37 expression was analyzed by IHC
364 staining. The results showed that TIPE expression was positively
365 correlated with PKM2 Ser37 expression ($P < 0.001$) (**Fig.7C, D**).

366 Consistent with the above findings, immunohistochemistry (IHC)
367 results showed that TIPE, PKM2 Ser37, LDH, and CSCs marker CD44
368 were inhibited in A375 TIPE-interfering cell-derived xenografts (**Fig.7E**).
369 Lastly, TCGA dataset revealed that TIPE has a positive relationship with
370 CSCs markers including *BMI1*, *NANOG*, *NOTCH1*, and
371 *OCT3/4*(*POU5F1*) in melanoma (**Fig.7F-I**).

372 These results further demonstrate that TIPE maintains cancer stem cell
373 phenotypes in a PKM2 dimerization manner.

374

375 Discussion

376 Accumulating evidence has revealed that TIPE serves as an oncogene and
377 a negative regulator of apoptosis. Its overexpression is positively
378 associated with the development of various cancers, including liver, lung,
379 and breast cancers(Lou et al., 2022; Niture et al., 2018). However, Chen
380 et al. reported that TIPE initially inhibits cancer cell proliferation but

381 promotes tumor migration and metastasis(Li et al., 2021). In addition, a
382 previous report has demonstrated that TIPE functions as a tumor
383 suppressor in certain inflammatory carcinogenesis(Lou et al., 2022).
384 These results suggest that TIPE plays a variety of roles in cancer
385 progression. Interestingly, Niture et al. reported that TIPE promotes
386 prostate cancer progression by regulating oxidative phosphorylation and
387 glycolysis(Niture et al., 2021). However, the mechanism through which
388 TIPE regulates metabolic reprogramming remains unclear. Here, we
389 demonstrate that TIPE facilitates the Warberg effect by promoting
390 dimeric PKM2-mediated HIF-1α transactivation in melanoma. Therefore,
391 targeting TIPE may offer a novel therapeutic approach for melanoma
392 treatment.

393 Mammalian pyruvate kinase consists of four isoforms, M1, M2, L, and
394 R, which are encoded by two distinct genes (PKM and PKLR) (Valentini
395 et al., 2002). Although these isoforms share similar features, only PKM2
396 exhibits the lowest basal enzymatic activity and is capable of
397 configuration transformation between the tetramer and dimer, meeting
398 differential metabolic demands(Morgan et al., 2013; Puckett et al., 2021).
399 Cancer cells shift towards the preferential expression of the specific
400 isoform of PKM2, especially its dimeric form, and serve as a pivotal
401 metabolic enzyme that promotes the activation of oncogenic pathways in
402 tumors(Icard et al., 2022). Normally, PKM2 enzymatic activity is

accurately modulated in a variety of ways, such as post-translational modifications or metabolite binding, to maintain balanced levels in tumor cells(Puckett et al., 2021). Here, we showed that TIPE promoted melanoma tumorigenesis by promoting glycolysis. The results showed that TIPE interacts with PKM2 and may participate in glycolysis. However, TIPE did not influence the expression of PKM2 at either the mRNA or the protein level. Because of the modulation of PKM2 kinetic properties primarily via its dimer and tetramer configurations, we demonstrated that TIPE could promote its dimeric form transformation, increasing PKM2 residing in the nucleus. However, the downstream signaling pathways that are mediated by TIPE in melanoma remain largely unknown.

The nuclear PKM2 routinely serves as a coactivator to transcriptionally activate certain metabolic genes(Cluntun et al., 2017; Zhang et al., 2019). Because TIPE binds PKM2 and transports it into the nucleus, the dimeric form of PKM2 more easily enters the nucleus to become a coactivator of HIF-1α, resulting in the upregulation of HIF-1α targeted genes such as *LDHA* and, *GLUT1*. Thus, we elucidate these relationships in the next step. To verify whether TIPE activates HIF-1α transcriptional activity, we found that TIPE significantly increased the activation of the HRE promoter, especially when combined with PKM2. However, this activation was diminished by interfering with PKM2, indicating that

425 TIPE has critical effects on the activation of HIF-1α transcription in a
426 PKM2-dependent manner. Because PKM2 interacts with HIF-1α and
427 potentiates PKM2-mediated HIF-1α transcription, we found that TIPE
428 increased the interaction between HIF-1α and PKM2. In TCGA dataset,
429 the hypoxia score was positively correlated with the mRNA expression of
430 TIPE in melanoma, and the TIPE higher expression group had a higher
431 hypoxia score than the lower expression group.

432 The mechanisms associated with PKM2 translocation are diverse, the
433 most important of which is Erk1/2-dependent phosphorylation of PKM2
434 at serine 37 (Ser37) and FGFR1-dependent phosphorylation of PKM2 at
435 tyrosine 105 (Tyr105)(Li et al., 2016; Zhou et al., 2018). Consequently,
436 we demonstrated that TIPE increased the levels of PKM2 Ser37 but not
437 PKM2 Tyr105. Furthermore, we conjectured that this transformation
438 caused by Ser37 phosphorylation affects the interaction between TIPE
439 and PKM2. The results showed that mutation of PKM2 at S37A blocked
440 its interaction with TIPE but not with Y105D. Because phosphorylation
441 of PKM2 at serine 37 is dependent on ERK1/2(Yang et al., 2012) and
442 TIPE promotes AML chemoresistance by activating the ERK signaling
443 pathway(Pang et al., 2020), we used an ERK inhibitor to further
444 demonstrate the activation of HIF-1αinduced by TIPE. Not surprisingly,
445 we found that TIPE facilitates the Warberg effect predominantly by
446 driving PKM2 Ser37 phosphorylation. Furthermore, we demonstrated

447 that the augmentation of TIPE on HRE promoter activation or HIF-1α
448 targeted genes such as *LDHA* and *GLUT1* was blocked by the S37A
449 mutation, as previously reported. These results demonstrated that TIPE
450 promotes HIF-1α transcriptional activation via ERK-dependent PKM2
451 Ser37 phosphorylation.

452 Increasing evidence has shown that HIF-1α promotes tumor
453 progression, metastasis, and therapeutic drug resistance by maintaining
454 cancer stemness(Cui et al., 2017; Niu et al., 2021). Here, we observed
455 that TIPE significantly enhanced tumorigenesis, glycolysis, and CSC
456 properties under normoxia in melanoma, whereas suppression of PKM2
457 dimerization rescued these TIPE-induced effects. Interestingly, we
458 revealed that decreasing of PKM2 dimerization can rescue TIPE induced
459 cell proliferation, glycolysis, and CSC properties. However, this
460 phenomenon was diminished by activation of HIF-1α, demonstrating that
461 TIPE promotes melanoma cells proliferation, glycolysis, and CSC
462 properties via dimeric PKM2 dependent HIF-1α activation. Furthermore,
463 using a tissue ship, we showed that the expression of TIPE in melanoma
464 tissues was dramatically increased compared to that in benign skin tumor
465 tissues. To determine if there was a correlation between TIPE and PKM2
466 Ser37 levels, the results also demonstrated that TIPE expression was
467 positively correlated with PKM2 Ser37 levels. Consistently, the
468 expression of TIPE has a positive relationship with PKM2 Ser37, LDH,

469 and the CSCs marker CD44 in TIPE-overexpressing cell-derived
470 xenografts. TCGA dataset revealed that TIPE has a positive relationship
471 with CSCs markers, including BMI1, NANOG, NOTCH1, and
472 OCT3/4(POU5F1) in melanoma. These results further demonstrate that
473 TIPE maintains melanoma cell stem phenotypes in a PKM2 dimerization
474 manner.

475 In summary, we identified that TIPE serves as an oncogenic candidate
476 for melanoma and determined that TIPE promotes the Warburg effect and
477 maintains the stemness of melanoma. TIPE binds to PKM2, inducing its
478 dimeric transformation by enhancing ERK-dependent PKM2 Ser37
479 phosphorylation, and thus activating the transcription of HIF-1α,
480 providing tumorigenicity and cancer stem-like phenomena for melanoma
481 progression. The newly identified TIPE/PKM2/HIF-1α axis is an ideal
482 therapeutic target for melanoma and opens an avenue for the development
483 of a novel strategy for precision therapy.

484

485 Materials and methods

486 Cell culture and plasmids construction

487 Human A375, A875, G361, MM96L and HEK-293T cell lines were
488 purchased from the Shanghai Institute of Cell Biology (Chinese Academy
489 of Sciences, Shanghai, China) and were maintained in Dulbecco's
490 modified Eagle's medium (DMEM, Gibco) supplemented with 10% fetal

491 bovine serum (FBS, Gibco) at 37°C under 5% CO_2. The TIPE
492 overexpression lentiviral vector (TIPE), TIPE expression knockdown
493 vector (TIPE-sh) and their control vectors were constructed by
494 GeneChem company (Shanghai, China). HIF-1α, PKM2-Flag, TIPE-HA
495 and their truncated vectors were constructed in our laboratory. The mutant
496 vectors such as PKM2 S37A were synthesized by Tsingke Biology Co.,
497 Ltd.(Beijing, China). All plasmids were transfected into the cells
498 according to the manufacturer's protocol.

499 **Cell proliferation, cell cycle and colony formation assays**

500 Cell proliferation was measured using the Cell Counting Kit-8 method
501 (Dojindo, Shanghai, China). For the cell cycle assay, the cells were
502 stained with propidium iodide (PI; Sigma, USA) and were measured with
503 a flow cytometer (FACS Aria 2, BD, USA). For the colony formation
504 assay, cells were seeded, fixed and stained as previously described(Yang
505 et al., 2022).

506 **Transwell assay**

507 Tranwell assay was performed as we previous described(Yang et al.,
508 2022). Photographs of at least three randomly selected fields were
509 captured and were counted.

510 **Bioinformatics, transcriptomics and metabolomics analyses**

511 The correlations between TIPE and HIF1A, Hypoxia score, cancer stem
512 cells (CSCs) markers including *BMI1*, *NANOG*, *NOTCH1* and

513 *OCT3/4*(*POU5F1*) were estimated by using the ASSISTANT for Clinical
514 Bioinformation website (https://www.aclbi.com/static/index.html#/).
515 Transcriptomics and metabolomics were performed and analyzed by
516 GeneChem company (Shanghai, China). Overexpression of TIPE into
517 G361 cells, interfering TIPE in A375 cells and their control group were
518 randomly divided into three groups to perform transcriptomic analyses,
519 respectively. Interfering TIPE in A375 cells and its control group were
520 randomly divided into six groups to perform metabolomic analyses.

521 **ATP content, ATPase activity, pyruvate kinase activity and lactic acid**
522 **content measurement**

523 The concentration of ATP was determined 72h after overexpression or
524 interfering of TIPE by using an ATP assay kit (Beyotime, S0026)
525 according to the manufacturer's instructions. ATPase activity was
526 measured by using an ATPase Assay Kit (Sigma-Aldrich, MAK113).
527 Pyruvate kinase activity and lactate production after overexpression or
528 interfering of TIPE were measured using a Pyruvate Kinase Activity
529 Assay Kit (Nanjing Jiancheng, A076-1-1) and Lactic Acid Assay Kit
530 (Nanjing Jiancheng, A019-2-1) according to the manufacturer's
531 instruction, respectively.

532 **ECAR**

533 The Extra Cellular Acidification Rate (ECAR) of melanoma cells were
534 determined using the Seahorse XF extracellular flux analyzer (Agilent,

535 Santa Clara, CA, USA). The cells were plated, washed before analysis.
536 The cells were then treated at specific time points: glucose (10 mM),
537 followed by oligomycin (1 μM) and 2-DG (50 mM). Finally, the ECAR
538 were measured by the Seahorse XF software.

539 **Chromatin Immunoprecipitation (ChIP) Quantitative PCR (ChIP-**
540 **qPCR)**

541 Melanoma cells were cross-linked with 1% formaldehyde, lysed with
542 sodium dodecyl sulfate buffer and sonicated. Sheared DNA was
543 immunoprecipitated with PKM2 antibody and negative control anti-IgG,
544 and quantified using SYBR Green Realtime PCR analysis (ABI, USA).
545 Primer sequences are listed in **Table S5**. Fold enrichment was calculated
546 based on Ct as $2^{-\Delta(\Delta Ct)}$, where $\Delta Ct = Ct_{IP} - Ct_{Input}$ and $\Delta(\Delta Ct) = \Delta Ct_{antibody} -$
547 ΔCt_{IgG}.

548 **Sphere formation assay**

549 Melanoma cells transfected with TIPE or TIPE-sh were plated onto 24-
550 well low attachment surface polystyrene plates (Corning, USA). Cells
551 were grown in DMEM/F12 medium (Invitrogen, USA) for approximately
552 10 days supplemented with 20ng/mL EGF (Bioworld, BK0026), 2% B27
553 (Invitrogen, 17504044), 20 ng/mL basic FGF (PeproThech, #100-18B),
554 and 1% N2(Invitrogen, 17502048).

555 **Luciferase reporter assay**

556 Human HEK-293T cells were seeded onto 48-well plates and transiently

557 transfected with pHRE-Firefly luciferase reporter, TIPE-HA and PKM2-
558 Flag or sh-RNA vector targeting PKM2 plasmids together with internal
559 control reporter pTK (Thymidine kinase)-Renilla luciferase by
560 Lipofectamine™ 2000 reagent (Thermo, USA). FLuc and RLuc activities
561 were determined using the Dual-Luciferase Assay System (Promega,
562 USA).

563 ***q*PCR**

564 mRNA was isolated and cDNAs were synthesized by using a Prime
565 Script RT Reagent Kit (TaKaRa, China) according to manufacturer's
566 instruction. *q*PCR was performed using Real SYBR Mixture (CoWin
567 Bioscience, China) on an ABI PRISM 7500 instrument (ThermoFisher,
568 USA). The sequences of the primers used in this study are listed in **Table**
569 **S5**.

570 **Duolink proximity ligation assay (PLA)**

571 Duolink® In Situ PLA® kit (Sigma-Aldrich, DUO92101) was performed
572 to demonstrate the endogenous interactions between TIPE and PKM2,
573 and to interpret how TIPE impact the interactions between HIF-1α and
574 PKM2 according to we described previously(Yang et al., 2022; Zhao et
575 al., 2019). Quantification analysis was performed using the ImageJ
576 software.

577 **Nuclear and cytosolic fractionation**

578 Nuclear and cytosolic fractions were prepared using NE-PER Extraction

579 Reagents (Thermo, 78833) according to the manufacturer's
580 recommendation. Finally, both cytosolic and nuclear subfractions were
581 stored in -80°C prior to western blot.

582 **Western blot**

583 The prepared lysates were separated by 10% sodium dodecyl sulfate
584 polyacrylamide gel electrophoresis and transferred onto PVDF
585 membranes (Bio-Rad, USA). The membranes were then blocked and
586 incubated overnight at 4°C with the primary antibodies (as listed in **Table**
587 **S6**). After incubated with secondary antibodies, the protein bands were
588 visualized using a Tanon 5200 Imager (Shanghai, China).

589 **Immunohistochemical and immunofluorescence**

590 Melanoma tissue chip was purchased from Zhongke Guanghua (Xi'an,
591 China) Intelligent Biotechnology Co., Ltd.(#K063Me01), and the
592 clinicopathological characteristics of melanoma specimens are
593 summarized in **Table S7**. Immunohistochemistry (IHC) staining was
594 performed as previously reported. The samples were finally analyzed by
595 using semiquantitative scoring criteria. The staining index values (0-12)
596 were obtained and calculated(Yang et al., 2022). For
597 immunofluorescence, cells were seeded onto 24-well plates at a density
598 of 5,000 cells per well. Then, the cells were fixed using 4% formaldehyde
599 solution and permeabilized with 0.5% Triton X-100 solution. Finally,
600 cells were incubated overnight with antibodies prior to blocked with 1%

601 bovine serum albumin (BSA) in phosphate-buffered saline containing
602 0.2% Tween-20. The fluorescence images of the cells were acquired with
603 a fluorescence microscope equipped with appropriate filter combinations.

604 **Co-immunoprecipitation (Co-IP) and Co-immunoprecipitation mass**
605 **spectrometry (Co-IP/MS)**

606 For Co-IP, the cells were seeded, harvested, and were then washed twice
607 with PBS and digested and lysed in lysis buffer. The lysed supernatant
608 was incubated with Tag-conjugated beads to bait the potential interacted
609 proteins according to the manufacturer's instruction. For Co-IP/MS, the
610 beads consequently were washed, eluted, resolved, and then stained with
611 Coomassie brilliant blue. The bands were excised and digested with
612 chymotrypsin and subjected to LC-MS/MS sequencing and data analysis
613 by OBiO Technology Corp.,Ltd. (Shanghai, China).

614 **Flow Cytometry Analysis**

615 Cell apoptosis was measured by using a Cell Apoptosis Analysis Kit
616 (Engreen Biosystem Co, Ltd., Beijing, China). The cells were then
617 incubated in serum-free medium for starvation prior to analysis and fixed
618 using 70% ethanol for 12 h. Consequently, cells were washed, incubated
619 with propidium iodide, and analyzed by a FACS scanner (Aria II, BD,
620 USA). For CD44 analyzing, the cells were seeded, harvested, and
621 incubated with anti-CD44 fluorescent antibody. Isotype-matched human
622 immunoglobulins served as controls. Finally, the cells were counted with

623 the FACS scanner.

624 **Mouse xenograft tumor study**

625 Xenograft tumor studies were conducted utilizing the 6-week-old male
626 BALB/c nude mice purchased from the Shanghai SLAC Laboratory
627 Animal Co., Ltd.. The total number of mice was randomly divided into
628 respective groups and maintained in a standard pathogen free
629 environment. All the animal experiments were approved by the Animal
630 Ethics Committee of Zibo Central Hospital, Binzhou Medical University.
631 Tumor growth was monitored regularly and the length, width, and height
632 measurements taken every 7 days. All mice were killed by 10 weeks post
633 injection. For the rescue test, one week after injection, mice bearing
634 TIPE-vector were treated with TEPP-46. TEPP-46 (50mg/kg) or vehicle
635 control (0.9% NaCl) was administrated via intraperitoneal injection. At
636 the end of experiment, mice were euthanized and tumors were collected.
637 Tumors were fixed with 4% paraformaldehyde for further
638 immunohistochemistry (IHC) analysis.

639 **Statistical analysis**

640 GraphPad Prism (GraphPad Software, San Diego, CA) was used for
641 statistical analyses. Two-tailed Student's t-tests were used to compare two
642 groups. Linear regression analysis was explored to analyze the correlation
643 of TIPE with other indicators. All the data are shown as the mean with
644 standard deviations (SD) from at least three independent experiments. A

645 *P* value of <0.05 was considered statistically significant for all tests.

646

647 **Data availability Statement**

648 All the data needed to evaluate the conclusions of the study are presented
649 in this paper. Additional data related to this study may be requested from
650 the corresponding author.

651 **Acknowledgements**

652 This work was supported by the National Natural Science Foundation of
653 China (Nos. 81972002, 12304241, 81971491), Natural Science
654 Foundation of Shandong Province (ZR2023QC68, ZR2023MC136,
655 ZR2021MC083, ZR2021MC165), Medicine and Health Science
656 Technology Development Projects of Shandong Province (202102050803
657 and 2018WS534), and Qingdao Postdoctoral Application Innovation
658 Project (QDBSH20230102068).

659 **Ethics approval**

660 This study has been approved by the Medical Ethics Committee, the
661 Animal Care and Use Committee of Zibo Central Hospital, Binzhou
662 Medical University.

663 **Author contributions**

664 Peiqing Zhao: Conceptualization, Supervision. Jianxin Du: Methodology,
665 Writing-Original draft preparation. Maojin Tian: Data curation,
666 Investigation. Le Yang: Investigation. Ziqian Zhao: Investigation. Jigang

Li: Validation. Qingqing Yin: Software. Lianqing Wang: Data curation. Wei Hu: Investigation. Yunwei Lou: Visualization.

Declaration of competing interest

The authors declare that they have no conflicts of interest concerning this article.

References

Baik, S.H., S. Kang, W. Lee, H. Choi, S. Chung, J.I. Kim, and I. Mook-Jung. 2019. A Breakdown in Metabolic Reprogramming Causes Microglia Dysfunction in

689 Alzheimer's Disease. *Cell Metab*. 30:493-507 e496.

690 Brunner, J.S., and L.W.S. Finley. 2022. Metabolic determinants of tumour initiation. *Nat Rev*
691 *Endocrinol*.

692 Chen, C., W. Zhang, T. Zhou, Q. Liu, C. Han, Z. Huang, S. Chen, Q. Mei, C. Zhang, K. Zhang,
693 H. Ma, R. Zhou, W. Jiang, W. Pan, and S. Zhu. 2022a. Vitamin B5 rewires Th17 cell
694 metabolism via impeding PKM2 nuclear translocation. *Cell Rep*. 41:111741.

695 Chen, Y., C. Cattoglio, G.M. Dailey, Q. Zhu, R. Tjian, and X. Darzacq. 2022b. Mechanisms
696 governing target search and binding dynamics of hypoxia-inducible factors. *Elife*. 11.

697 Christofk, H.R., M.G. Vander Heiden, N. Wu, J.M. Asara, and L.C. Cantley. 2008. Pyruvate
698 kinase M2 is a phosphotyrosine-binding protein. *Nature*. 452:181-186.

699 Cluntun, A.A., M.J. Lukey, R.A. Cerione, and J.W. Locasale. 2017. Glutamine Metabolism in
700 Cancer: Understanding the Heterogeneity. *Trends Cancer*. 3:169-180.

701 Cui, C.P., C.C. Wong, A.K. Kai, D.W. Ho, E.Y. Lau, Y.M. Tsui, L.K. Chan, T.T. Cheung, K.S.
702 Chok, A.C.Y. Chan, R.C. Lo, J.M. Lee, T.K. Lee, and I.O.L. Ng. 2017. SENP1
703 promotes hypoxia-induced cancer stemness by HIF-1alpha deSUMOylation and
704 SENP1/HIF-1alpha positive feedback loop. *Gut*. 66:2149-2159.

705 D'Aguanno, S., F. Mallone, M. Marenco, D. Del Bufalo, and A. Moramarco. 2021. Hypoxia-
706 dependent drivers of melanoma progression. *J Exp Clin Cancer Res*. 40:159.

707 Dhanesha, N., R.B. Patel, P. Doddapattar, M. Ghatge, G.D. Flora, M. Jain, D. Thedens, H.
708 Olalde, M. Kumskova, E.C. Leira, and A.K. Chauhan. 2022. PKM2 promotes
709 neutrophil activation and cerebral thromboinflammation: therapeutic implications for
710 ischemic stroke. *Blood*. 139:1234-1245.

711 Faubert, B., A. Solmonson, and R.J. DeBerardinis. 2020. Metabolic reprogramming and
712 cancer progression. *Science*. 368.
713 Goldsmith, J.R., S. Fayngerts, and Y.H. Chen. 2017. Regulation of inflammation and
714 tumorigenesis by the TIPE family of phospholipid transfer proteins. *Cell Mol Immunol*.
715 14:482-487.
716 Guo, D., Y. Tong, X. Jiang, Y. Meng, H. Jiang, L. Du, Q. Wu, S. Li, S. Luo, M. Li, L. Xiao, H.
717 He, X. He, Q. Yu, J. Fang, and Z. Lu. 2022. Aerobic glycolysis promotes tumor
718 immune evasion by hexokinase2-mediated phosphorylation of IkappaBalpha. *Cell*
719 *Metab*. 34:1312-1324 e1316.
720 Han, A., Z.T. Schug, and A.E. Aplin. 2021. Metabolic Alterations and Therapeutic
721 Opportunities in Rare Forms of Melanoma. *Trends Cancer*. 7:671-681.
722 Hu, Y., and G.K. Smyth. 2009. ELDA: extreme limiting dilution analysis for comparing
723 depleted and enriched populations in stem cell and other assays. *J Immunol Methods*.
724 347:70-78.
725 Icard, P., L. Simula, L. Fournel, K. Leroy, A. Lupo, D. Damotte, M.C. Charpentier, C. Durdux,
726 M. Loi, O. Schussler, G. Chassagnon, A. Coquerel, H. Lincet, V. De Pauw, and M.
727 Alifano. 2022. The strategic roles of four enzymes in the interconnection between
728 metabolism and oncogene activation in non-small cell lung cancer: Therapeutic
729 implications. *Drug Resist Updat*. 63:100852.
730 Li, M., X. Li, J.R. Goldsmith, S. Shi, L. Zhang, A. Zamani, L. Wan, H. Sun, T. Li, J. Yu, Z.
731 Etwebi, M.J. Bou-Dargham, and Y.H. Chen. 2021. Decoupling tumor cell metastasis
732 from growth by cellular pilot protein TNFAIP8. *Oncogene*. 40:6456-6468.

733 Li, N., L. Feng, H. Liu, J. Wang, M. Kasembeli, M.K. Tran, D.J. Tweardy, S.H. Lin, and J.
734 Chen. 2016. PARP Inhibition Suppresses Growth of EGFR-Mutant Cancers by
735 Targeting Nuclear PKM2. *Cell Rep*. 15:843-856.
736 Liu, F., F. Ma, Y. Wang, L. Hao, H. Zeng, C. Jia, Y. Wang, P. Liu, I.M. Ong, B. Li, G. Chen, J.
737 Jiang, S. Gong, L. Li, and W. Xu. 2017. PKM2 methylation by CARM1 activates
738 aerobic glycolysis to promote tumorigenesis. *Nat Cell Biol*. 19:1358-1370.
739 Liu, F., M. Ma, A. Gao, F. Ma, G. Ma, P. Liu, C. Jia, Y. Wang, K. Donahue, S. Zhang, I.M.
740 Ong, S. Keles, L. Li, and W. Xu. 2021. PKM2-TMEM33 axis regulates lipid
741 homeostasis in cancer cells by controlling SCAP stability. *EMBO J*. 40:e108065.
742 Lou, Y., X. Tian, C. Sun, M. Song, M. Han, Y. Zhao, Y. Song, X. Song, W. Zhang, Y.H. Chen,
743 and H. Wang. 2022. TNFAIP8 protein functions as a tumor suppressor in
744 inflammation-associated colorectal tumorigenesis. *Cell Death Dis*. 13:311.
745 Luo, W., H. Hu, R. Chang, J. Zhong, M. Knabel, R. O'Meally, R.N. Cole, A. Pandey, and G.L.
746 Semenza. 2011. Pyruvate kinase M2 is a PHD3-stimulated coactivator for hypoxia-
747 inducible factor 1. *Cell*. 145:732-744.
748 Malekan, M., M.A. Ebrahimzadeh, and F. Sheida. 2021. The role of Hypoxia-Inducible Factor-
749 1alpha and its signaling in melanoma. *Biomed Pharmacother*. 141:111873.
750 Morgan, H.P., F.J. O'Reilly, M.A. Wear, J.R. O'Neill, L.A. Fothergill-Gilmore, T. Hupp, and
751 M.D. Walkinshaw. 2013. M2 pyruvate kinase provides a mechanism for nutrient
752 sensing and regulation of cell proliferation. *Proc Natl Acad Sci U S A*. 110:5881-5886.
753 Niture, S., X. Dong, E. Arthur, U. Chimeh, S.S. Niture, W. Zheng, and D. Kumar. 2018.
754 Oncogenic Role of Tumor Necrosis Factor alpha-Induced Protein 8 (TNFAIP8). *Cells*.

755 8.

756 Niture, S., M. Lin, J.O. Odera, J. Moore, H. Zhe, X. Chen, S. Suy, S.P. Collins, and D. Kumar.
757 2021. TNFAIP8 drives metabolic reprogramming to promote prostate cancer cell
758 proliferation. *Int J Biochem Cell Biol*. 130:105885.

759 Niu, J., W. Li, C. Liang, X. Wang, X. Yao, R.H. Yang, Z.S. Zhang, H.F. Liu, F.Y. Liu, S.H. Pei,
760 W.Q. Li, H. Sun, D. Fang, and S.Q. Xie. 2020. EGF promotes DKK1 transcription in
761 hepatocellular carcinoma by enhancing the phosphorylation and acetylation of
762 histone H3. *Sci Signal*. 13.

763 Niu, Y., Z. Lin, A. Wan, L. Sun, S. Yan, H. Liang, S. Zhan, D. Chen, X. Bu, P. Liu, C. Chen, W.
764 He, X. Lu, and G. Wan. 2021. Loss-of-Function Genetic Screening Identifies Aldolase
765 A as an Essential Driver for Liver Cancer Cell Growth Under Hypoxia. *Hepatology*.
766 74:1461-1479.

767 Novoyatleva, T., N. Rai, N. Weissmann, F. Grimminger, H.A. Ghofrani, W. Seeger, H. Gall,
768 and R.T. Schermuly. 2019. Is PKM2 Phosphorylation a Prerequisite for Oligomer
769 Disassembly in Pulmonary Arterial Hypertension? *Am J Respir Crit Care Med*.
770 200:1550-1554.

771 Ouyang, X., S.N. Han, J.Y. Zhang, E. Dioletis, B.T. Nemeth, P. Pacher, D. Feng, R. Bataller,
772 J. Cabezas, P. Starkel, J. Caballeria, R.L. Pongratz, S.Y. Cai, B. Schnabl, R. Hoque,
773 Y. Chen, W.H. Yang, I. Garcia-Martinez, F.S. Wang, B. Gao, N.J. Torok, R.G. Kibbey,
774 and W.Z. Mehal. 2018. Digoxin Suppresses Pyruvate Kinase M2-Promoted HIF-
775 1alpha Transactivation in Steatohepatitis. *Cell Metab*. 27:339-350 e333.

776 Padmavathi, G., K. Banik, J. Monisha, D. Bordoloi, B. Shabnam, F. Arfuso, G. Sethi, L. Fan,

777 and A.B. Kunnumakkara. 2018. Novel tumor necrosis factor-alpha induced protein
778 eight (TNFAIP8/TIPE) family: Functions and downstream targets involved in cancer
779 progression. *Cancer Lett*. 432:260-271.
780 Pang, Y., Y. Zhao, Y. Wang, X. Wang, R. Wang, N. Liu, P. Li, M. Ji, J. Ye, T. Sun, J. Li, D. Ma,
781 F. Lu, and C. Ji. 2020. TNFAIP8 promotes AML chemoresistance by activating ERK
782 signaling pathway through interaction with Rac1. *J Exp Clin Cancer Res*. 39:158.
783 Puckett, D.L., M. Alquraishi, W. Chowanadisai, and A. Bettaieb. 2021. The Role of PKM2 in
784 Metabolic Reprogramming: Insights into the Regulatory Roles of Non-Coding RNAs.
785 *Int J Mol Sci*. 22.
786 Valentini, G., L.R. Chiarelli, R. Fortin, M. Dolzan, A. Galizzi, D.J. Abraham, C. Wang, P.
787 Bianchi, A. Zanella, and A. Mattevi. 2002. Structure and function of human
788 erythrocyte pyruvate kinase. Molecular basis of nonspherocytic hemolytic anemia. *J*
789 *Biol Chem*. 277:23807-23814.
790 Wang, H.J., Y.J. Hsieh, W.C. Cheng, C.P. Lin, Y.S. Lin, S.F. Yang, C.C. Chen, Y. Izumiya,
791 J.S. Yu, H.J. Kung, and W.C. Wang. 2014. JMJD5 regulates PKM2 nuclear
792 translocation and reprograms HIF-1alpha-mediated glucose metabolism. *Proc Natl*
793 *Acad Sci U S A*. 111:279-284.
794 Wei, Y., M. Lu, M. Mei, H. Wang, Z. Han, M. Chen, H. Yao, N. Song, X. Ding, J. Ding, M. Xiao,
795 and G. Hu. 2020. Pyridoxine induces glutathione synthesis via PKM2-mediated Nrf2
796 transactivation and confers neuroprotection. *Nat Commun*. 11:941.
797 Weinstein, A.G., I. Godet, and D.M. Gilkes. 2022. The rise of viperin: the emerging role of
798 viperin in cancer progression. *J Clin Invest*. 132.

799 Yang, M., Y. Zhang, G. Liu, Z. Zhao, J. Li, L. Yang, K. Liu, W. Hu, Y. Lou, J. Jiang, Q. Liu,
800 and P. Zhao. 2022. TIPE1 inhibits osteosarcoma tumorigenesis and progression by
801 regulating PRMT1 mediated STAT3 arginine methylation. *Cell Death Dis*. 13:815.
802 Yang, W., Y. Zheng, Y. Xia, H. Ji, X. Chen, F. Guo, C.A. Lyssiotis, K. Aldape, L.C. Cantley,
803 and Z. Lu. 2012. ERK1/2-dependent phosphorylation and nuclear translocation of
804 PKM2 promotes the Warburg effect. *Nat Cell Biol*. 14:1295-1304.
805 Yang, Y.C., M.H. Chien, H.Y. Liu, Y.C. Chang, C.K. Chen, W.J. Lee, T.C. Kuo, M. Hsiao, K.T.
806 Hua, and T.Y. Cheng. 2018. Nuclear translocation of PKM2/AMPK complex sustains
807 cancer stem cell populations under glucose restriction stress. *Cancer Lett*. 421:28-40.
808 Zhang, Z., X. Deng, Y. Liu, Y. Liu, L. Sun, and F. Chen. 2019. PKM2, function and expression
809 and regulation. *Cell Biosci*. 9:52.
810 Zhao, P., X. Pang, J. Jiang, L. Wang, X. Zhu, Y. Yin, Q. Zhai, X. Xiang, F. Feng, and W. Xu.
811 2019. TIPE1 promotes cervical cancer progression by repression of p53 acetylation
812 and is associated with poor cervical cancer outcome. *Carcinogenesis*. 40:592-599.
813 Zhou, Q., Y. Yin, M. Yu, D. Gao, J. Sun, Z. Yang, J. Weng, W. Chen, M. Atyah, Y. Shen, Q.
814 Ye, C.W. Li, M.C. Hung, Q. Dong, C. Zhou, and N. Ren. 2022. GTPBP4 promotes
815 hepatocellular carcinoma progression and metastasis via the PKM2 dependent
816 glucose metabolism. *Redox Biol*. 56:102458.
817 Zhou, Z., M. Li, L. Zhang, H. Zhao, O. Sahin, J. Chen, J.J. Zhao, Z. Songyang, and D. Yu.
818 2018. Oncogenic Kinase-Induced PKM2 Tyrosine 105 Phosphorylation Converts
819 Nononcogenic PKM2 to a Tumor Promoter and Induces Cancer Stem-like Cells.
820 *Cancer Res*. 78:2248-2261.

821 Zhu, B., W. Zhong, X. Cao, G. Pan, M. Xu, J. Zheng, H. Chen, X. Feng, C. Luo, C. Lu, J. Xiao,
822 W. Lin, C. Lai, M. Li, X. Du, Q. Yi, and D. Yan. 2022. Loss of miR-31-5p drives
823 hematopoietic stem cell malignant transformation and restoration eliminates leukemia
824 stem cells in mice. *Sci Transl Med*. 14:eabh2548.

825

826

827

828

829

830

831

832

833

834

835

836

837

838

839

840

841

842

843

844

845

846 **Figure Legends**

847 **Figure 1. Effect of TIPE on melanoma cell glycolysis. A, B.**
848 Transcriptomics analysis by unsupervised hierarchical clustering and
849 Kyoto Encyclopedia of Genes and Genomes (KEGG) analysis showed
850 that TIPE increased glycolysis and HIF-1α pathways. **C.** GSEA analysis
851 of glycolysis showed that TIPE enhanced glycolysis compared to the
852 control. **D.** Untargeted metabolomics analysis indicated that interfering
853 with TIPE decreased the glycolysis pathway. **E-G.** TIPE decreases
854 ATPase activity and ATP content and increases lactate levels. **H, I.**
855 Overexpression of TIPE promotes glycolysis and glycolytic capacity
856 according to ECAR analysis. **J, K.** Interfering with TIPE decreased
857 glycolysis and glycolytic capacity using ECAR analysis. **L.** TIPE
858 significantly activated HRE activity. *P<0.05; **P<0.01; ***P<0.001.

859

860 **Figure 2. TIPE interacts with PKM2 to govern its nuclear import in a**
861 **dimeric form dependent manner. A.** Co-IP/MS analysis demonstrated
862 that PKM2 interacted with TIPE in A375 cells. **B, C.**
863 Immunoprecipitation (IP) and western blot analysis of the exogenous
864 TIPE/PKM2 proteins interaction in the HEK-293T cells co-transfected

865 with Flag-tagged PKM2 and HA-tagged TIPE. **D, E.** IP and western blot
866 analysis of the endogenous TIPE/PKM2 proteins interaction in the A375
867 cells. **F.** GST-pull down assay analysis of TIPE/PKM2 proteins
868 interaction using purified GST-tagged PKM2 and TIPE-HA. **G.** TIPE
869 (rabbit source, $TIPE_R$) endogenously interacted with PKM2(mouse
870 source, $PKM2_M$) in G361 cells by using the Doulink assay. The results
871 suggested that TIPE interacted with PKM2 to form a red color complex.
872 The red color signal is generated only when the two proteins are too close
873 to interaction. **H, I.** IP and western blot analysis of HA-tagged TIPE and
874 Flag-tagged PKM2 fragment protein interaction in HEK-293T cells. **J.** IP
875 and western blot analysis of the Flag-tagged PKM2 and HA-tagged TIPE
876 fragment protein interaction in HEK-293T cells. **K.** Interfering TIPE
877 decreased PKM2 dimeric formation but increased tetramer formation, as
878 analyzed by BN-PAGE with β-actin as a loading control. **L.**
879 Overexpression of TIPE increased PKM2 dimeric formation and
880 decreased tetramer formation. **M.** Western blot showed that TIPE
881 promoted PKM2 translocation into the nucleus. **N.** TIPE enhanced PKM2
882 translocation into the nucleus, and this phenomenon was diminished by
883 the administration of TEPP-46 (100μM). *P<0.05; **P<0.01.
884
885 **Figure 3. TIPE promotes HIF-1α transcription in a PKM2-dependent**
886 **manner. A.** Proposed molecular mechanism by which dimeric PKM2

887 regulates cell proliferation and glycolysis by modulating HIF-1α activity.
888 **B.** TIPE, especially when combined with PKM2, boosts relative HRE
889 luciferase activity, as examined by luciferase reporter assay. **C.** TIPE
890 promoted HRE activity in a dose- and PKM2-dependent manner. **D, E.**
891 TIPE increases HIF-1α targeted genes, including *LDHA* and *GLUT1*, in a
892 dose- and PKM2-dependent manner. **F, G.** TIPE promoted endogenous
893 interaction between PKM2 and HIF-1α in melanoma cells using a
894 Doulink assay. Interference of TIPE in A375 cells promoted the
895 interaction between PKM2 and HIF-1α(upper) compared to that
896 overexpression of TIPE in G361 cells decreased their interaction (lower).
897 The density of the red color signaling means the interactive strength
898 between PKM2 and HIF-1α affected by TIPE. **H.** TIPE enhanced the
899 PKM2/HIF1a interaction in the nucleus. **I.** TIPE increased the exogenous
900 interaction between PKM2 and HIF-1α in a dose- dependent manner in
901 HEK-293T cells. **J.** TCGA dataset revealed that TIPE has a positive
902 relationship with hypoxia score in melanoma. **K.** Higher expression of
903 TIPE is associated with a relatively higher hypoxia score in melanoma.
904 *P<0.05; **P<0.01; ***P<0.001.
905
906 **Figure 4. TIPE increases HIF-1α activity depending on PKM2 Ser37**
907 **phosphorylation. A.** TIPE enhanced PKM2 Ser37 phosphorylation, but
908 not that of Tyr105. **B.** PKM2 Ser37, but not Tyr105, increased its

interaction with TIPE. **C.** PKM2 Ser37 mutation(S37A) hampered its interaction with HIF-1α promoted by TIPE. **D.** TIPE elevated PKM2 Ser37 phosphorylation in an ERK-dependent manner. **E, F.** TIPE enhanced PKM2 binding to the HRE for *LDHA* and *GLUT1* in a dimeric form dependent manner. **G.** PKM2 Ser37 mutation(S37A) inhibited the HRE activity induced by TIPE. **H, I.** PKM2 Ser37 mutation(S37A) decreased the expression of *LDHA* and *GLUT1* that promoted by TIPE. $^{**}P<0.01$; $^{***}P<0.001$.

Figure 5. TIPE promotes melanoma cells proliferation and glycolysis depending on PKM2 dimerization. A. Pyridoxine (which facilitates PKM2 dimerization) treatment reversed the inhibition of cell proliferation that induced via interfering TIPE. **B.** Administration of TEPP-46 rescued TIPE overexpression induced cell proliferation. **C, D.** TIPE promoted melanoma clone formation in a dimeric PKM2-dependent manner. **E-G.** *In vivo* experiments showed that TIPE promoted melanoma proliferation via the dimerization of PKM2. **H-J.** Activation of PKM2 dimerization reversed the inhibition of glycolysis and glycolytic capacity after TIPE interfering. In contrast, inhibition of PKM2 dimerization altered this phenomenon (**K-M**). **N.** Pyridoxine increased the cell proliferation that was inhibited by TIPE-sh. It was rescued by inhibition of HIF-1α. **O.** TEPP-46 inhibited the TIPE-induced cell proliferation, and was rescued

931 by overexpression of HIF-1α. **P.** Pyridoxine enhanced the Warberg effect
932 that was suppressed by TIPE-sh, and it was diminished via administration
933 of PX-478(a HIF-1α inhibitor). **Q.** TEPP-46 can suppression of the
934 Warberg effect that was increased by overexpression of TIPE, this
935 phenomenon was diminished by overexpression of HIF-1α. *P<0.05;
936 ***P<0.001.
937

938 **Figure 6. TIPE fostered PKM2 dimerization increases melanoma**
939 **stem-like phenomenon. A, B.** TIPE increased the cancer stem-like
940 phenotype markers, including *NANOG*, *NOTCH*, *OCT3/4*, *SOX2* and
941 *BMI-1*, measured by *q*PCR. **C-F.** The effects of TIPE on the stemness of
942 melanoma cells are shown by *in vitro* cell migration (**C**), sphere
943 formation (**D**), and chemoresistance (**E, F**). **G.** Limiting dilution
944 xenograft formation of A375 cells with TIPE interference. **H, I.** TIPE
945 increased the expression of $CD44^+$ cells in melanoma. **J, K.** The effects of
946 TIPE on the stemness of melanoma cells following the administration of
947 TEPP-46, and this phenomenon was reversed by overexpression of HIF-
948 1α, as evidenced by sphere formation (**J**) and $CD44^+$ cell population (**K**).
949 *P<0.05; **P<0.01; ***P<0.001.
950

951 **Figure 7. TIPE positively corelated with cancer stem cell markers**
952 **and the levels of p-PKM2(Ser37). A, B.** Higher expression of TIPE was

953 observed in melanoma tumor tissues than in the control, as evidenced by
954 immunohistochemistry. **C, D.** The expression of TIPE correlated well
955 with p-PKM2(Ser37) in melanoma tumor tissues. **E.** Similarly, a good
956 correlation was observed between TIPE, p-PKM2(Ser37), LDH, and
957 CD44 in mouse xenografts. **F-I.** In addition, the expression of TIPE was
958 positively correlated with CSCs markers, including *BMI1*, *NANOG*,
959 *NOTCH1*, and *OCT3/4*(*POU5F1*) in TCGA dataset. **J.** A brief model
960 depicting the functional impact of TIPE on metabolic reprogramming in
961 melanoma. ***$P<0.001$.

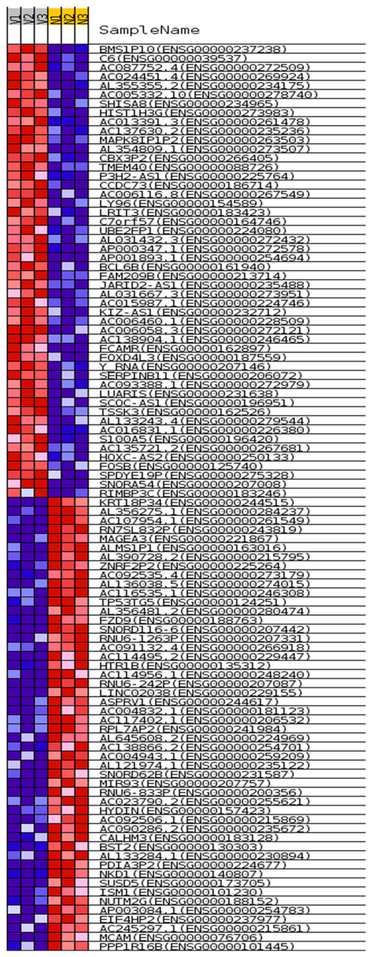
A
SampleName

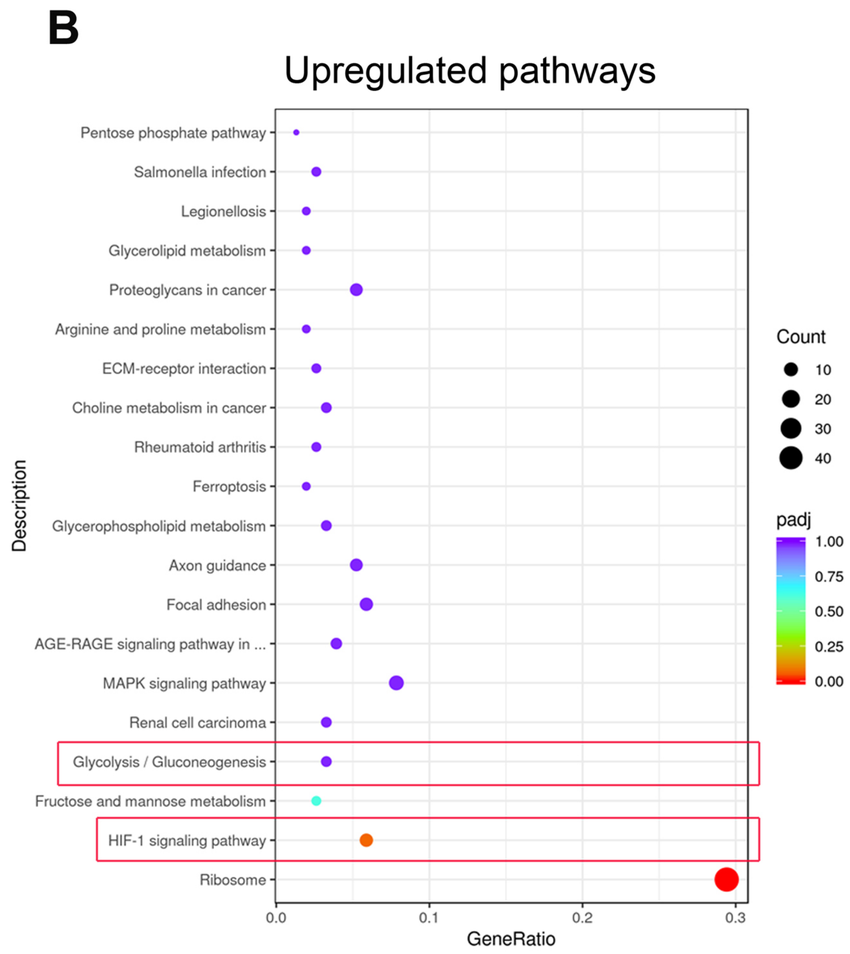
B
Upregulated pathways
Pentose phosphate pathway
Salmonella infection
Legionellosis
Glycerolipid metabolism
Proteoglycans in cancer
Arginine and proline metabolism
ECM-receptor interaction
Choline metabolism in cancer
Rheumatoid arthritis
Ferroptosis
Glycerophospholipid metabolism
Axon guidance
Focal adhesion
AGE-RAGE signaling pathway in ...
MAPK signaling pathway
Renal cell carcinoma
Glycolysis / Gluconeogenesis
Fructose and mannose metabolism
HIF-1 signaling pathway
Ribosome
Description
GeneRatio
Count
padj

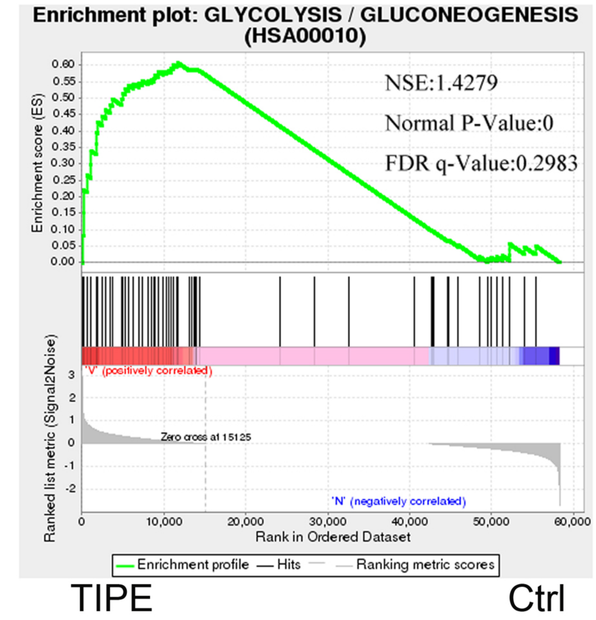
C
Enrichment plot: GLYCOLYSIS / GLUCONEOGENESIS (HSA00010)
NSE:1.4279
Normal P-Value:0
FDR q-Value:0.2983
Enrichment score (ES)
Ranked list metric (Signal2Noise)
Rank in Ordered Dataset
Enrichment profile
Hits
Ranking metric scores
TIPE
Ctrl

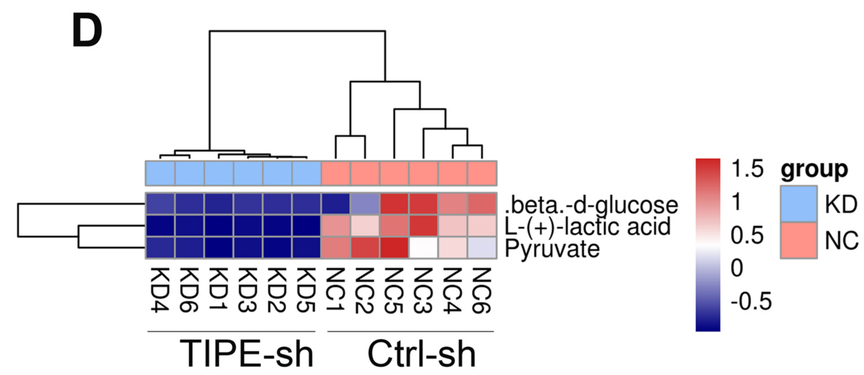
D
.beta.-d-glucose
L-(+)-lactic acid
Pyruvate
KD4
KD6
KD1
KD3
KD2
KD5
NC1
NC2
NC5
NC3
NC4
NC6
TIPE-sh
Ctrl-sh
group
KD
NC

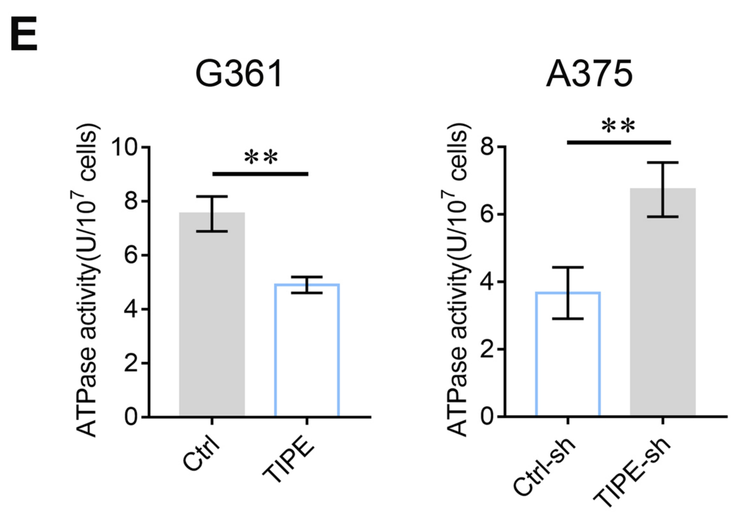
E
G361
A375
ATPase activity(U/10^7 cells)
Ctrl
TIPE
Ctrl-sh
TIPE-sh

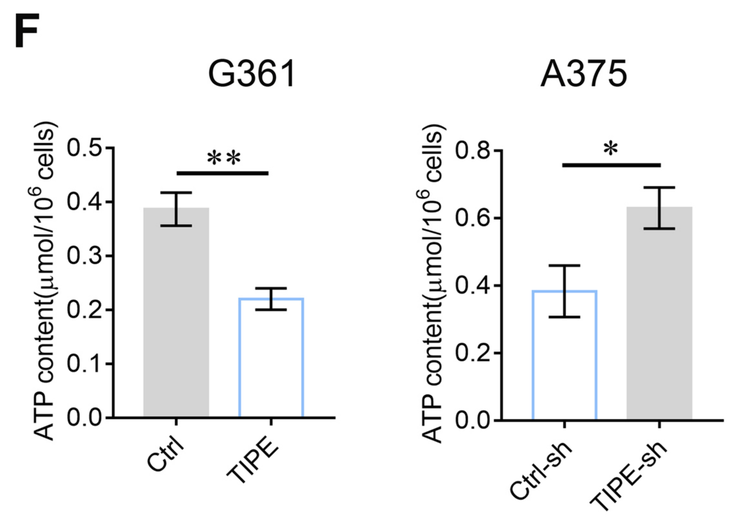
F
G361
A375
ATP content(μmol/10^6 cells)
Ctrl
TIPE
Ctrl-sh
TIPE-sh

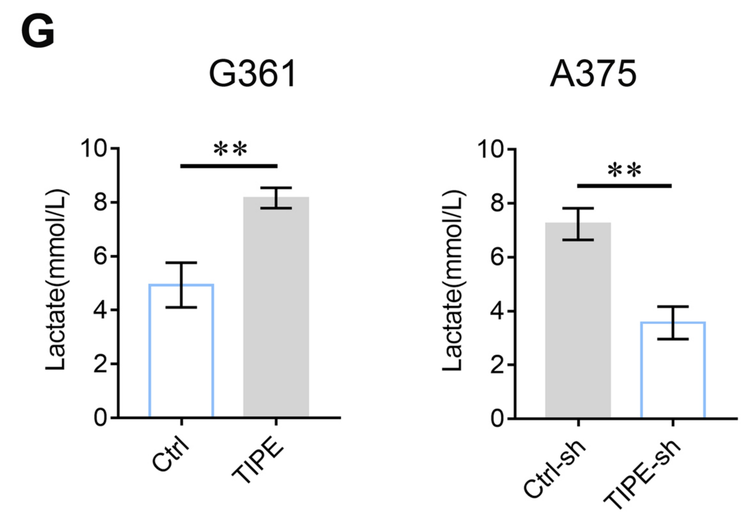
G
G361
A375
Lactate(mmol/L)
Ctrl
TIPE
Ctrl-sh
TIPE-sh

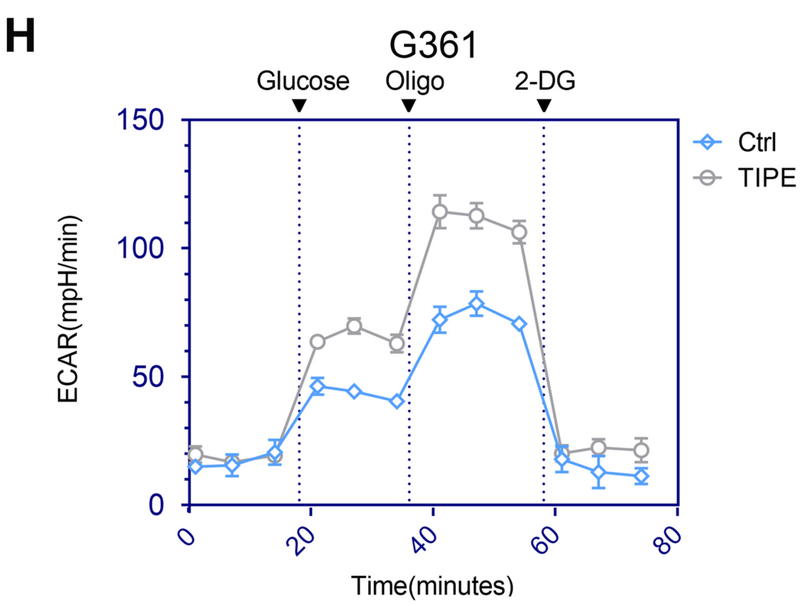
H
G361
Glucose
Oligo
2-DG
ECAR(mpH/min)
Time(minutes)
Ctrl
TIPE

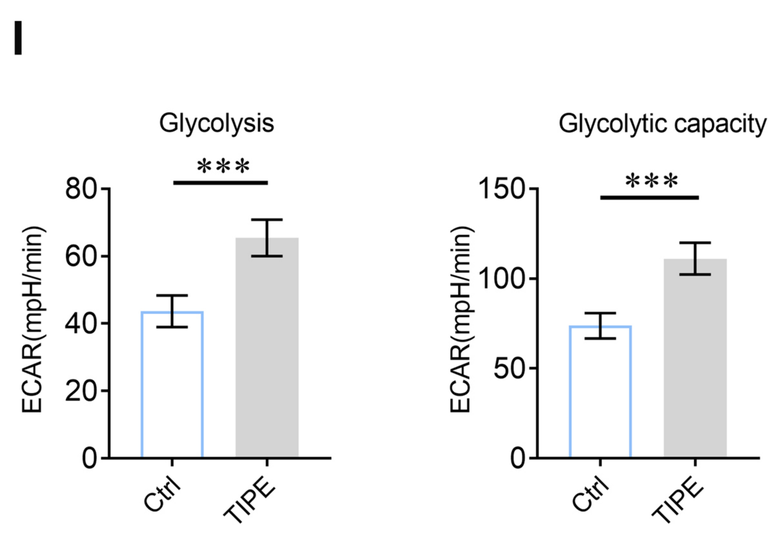
I
Glycolysis
Glycolytic capacity
ECAR(mpH/min)
Ctrl
TIPE

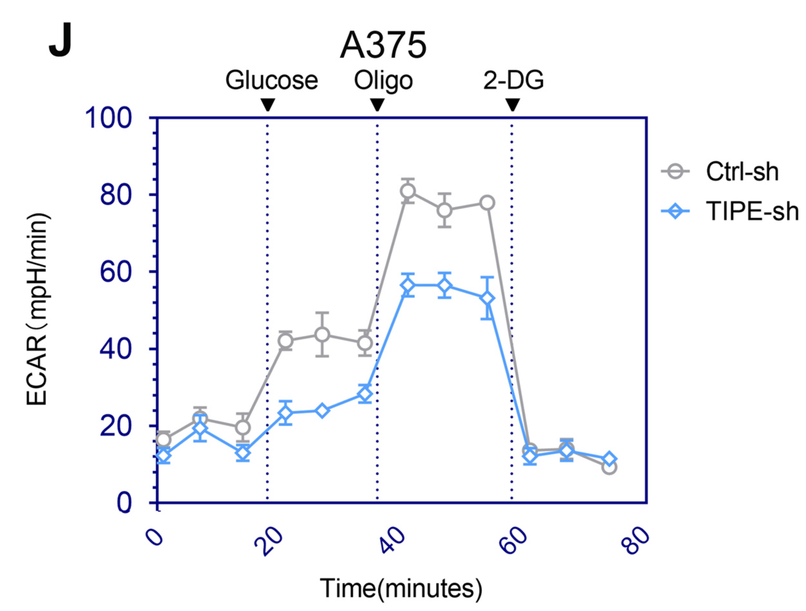
J
A375
Glucose
Oligo
2-DG
ECAR (mpH/min)
Time(minutes)
Ctrl-sh
TIPE-sh

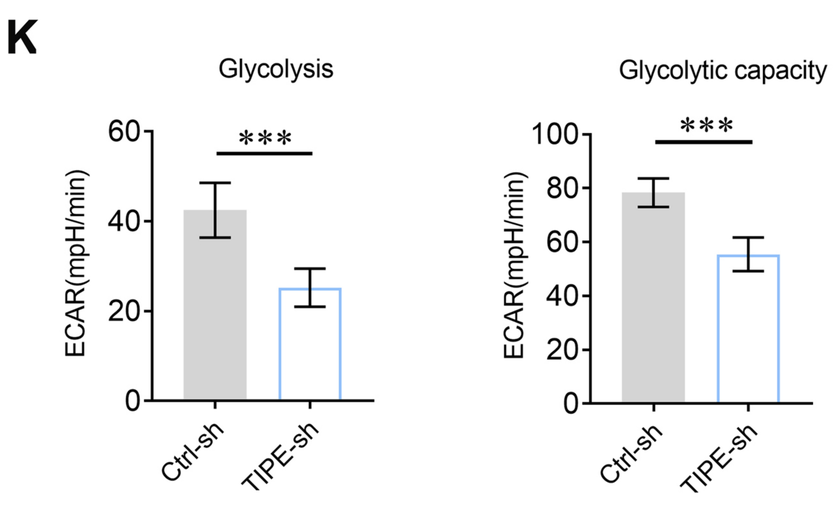
K
Glycolysis
Glycolytic capacity
ECAR(mpH/min)
Ctrl-sh
TIPE-sh

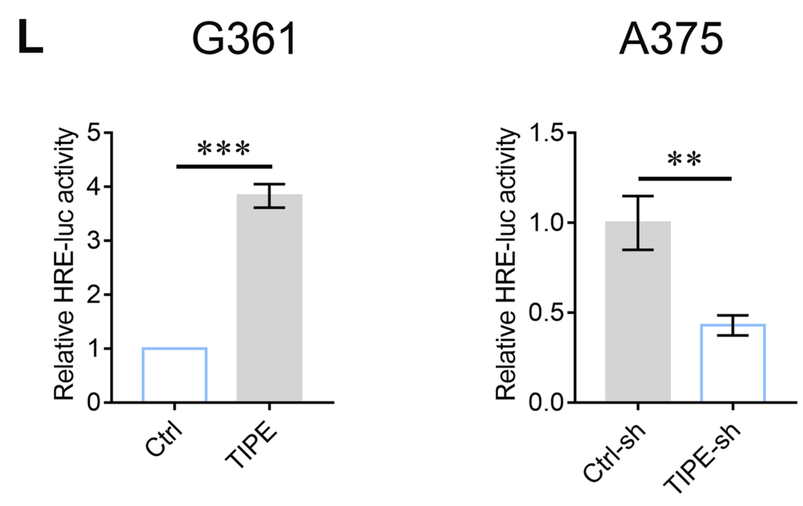
L
G361
A375
Relative HRE-luc activity
Ctrl
TIPE
Ctrl-sh
TIPE-sh

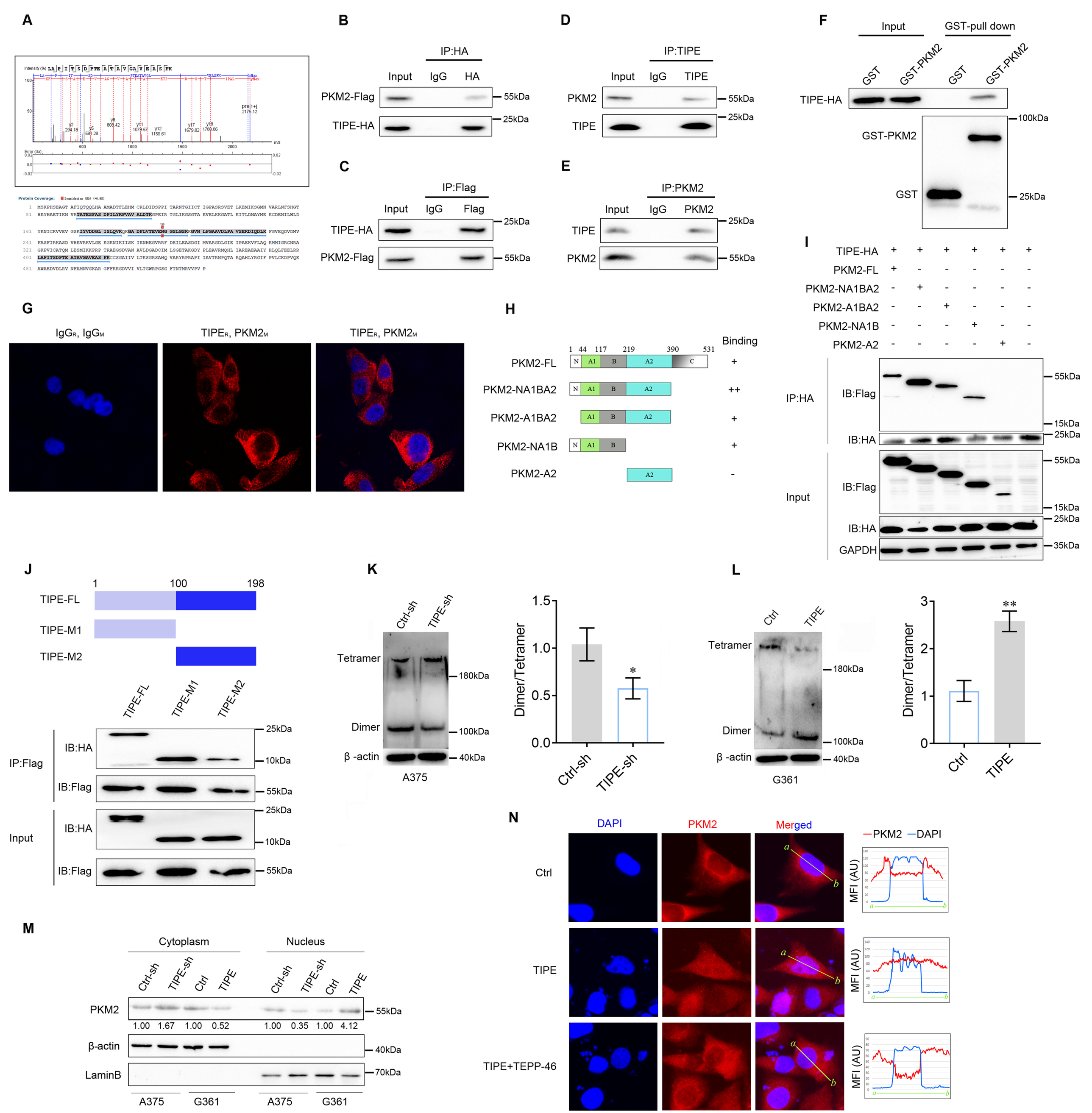
A
B
IP:HA
Input
IgG
HA
PKM2-Flag
TIPE-HA
55kDa
25kDa
C
IP:Flag
Input
IgG
Flag
TIPE-HA
PKM2-Flag
25kDa
55kDa
D
IP:TIPE
Input
IgG
TIPE
PKM2
TIPE
55kDa
25kDa
E
IP:PKM2
Input
IgG
PKM2
TIPE
PKM2
25kDa
55kDa
F
Input
GST-pull down
GST
GST-PKM2
GST
GST-PKM2
TIPE-HA
GST-PKM2
GST
100kDa
25kDa
G
IgGR, IgGM
TIPER, PKM2M
TIPER, PKM2M
H
Binding
PKM2-FL
PKM2-NA1BA2
PKM2-A1BA2
PKM2-NA1B
PKM2-A2
+
++
+
+
-
I
TIPE-HA
PKM2-FL
PKM2-NA1BA2
PKM2-A1BA2
PKM2-NA1B
PKM2-A2
IP:HA
IB:Flag
IB:HA
Input
GAPDH
55kDa
15kDa
25kDa
35kDa
J
TIPE-FL
TIPE-M1
TIPE-M2
IP:Flag
Input
IB:HA
IB:Flag
25kDa
10kDa
55kDa
K
Ctrl-sh
TIPE-sh
Tetramer
Dimer
β -actin
180kDa
100kDa
40kDa
A375
Dimer/Tetramer
L
Ctrl
TIPE
G361
M
Cytoplasm
Nucleus
PKM2
β-actin
LaminB
55kDa
40kDa
70kDa
1.00 1.67 1.00 0.52
1.00 0.35 1.00 4.12
A375
G361
N
DAPI
PKM2
Merged
Ctrl
TIPE
TIPE+TEPP-46
MFI (AU)

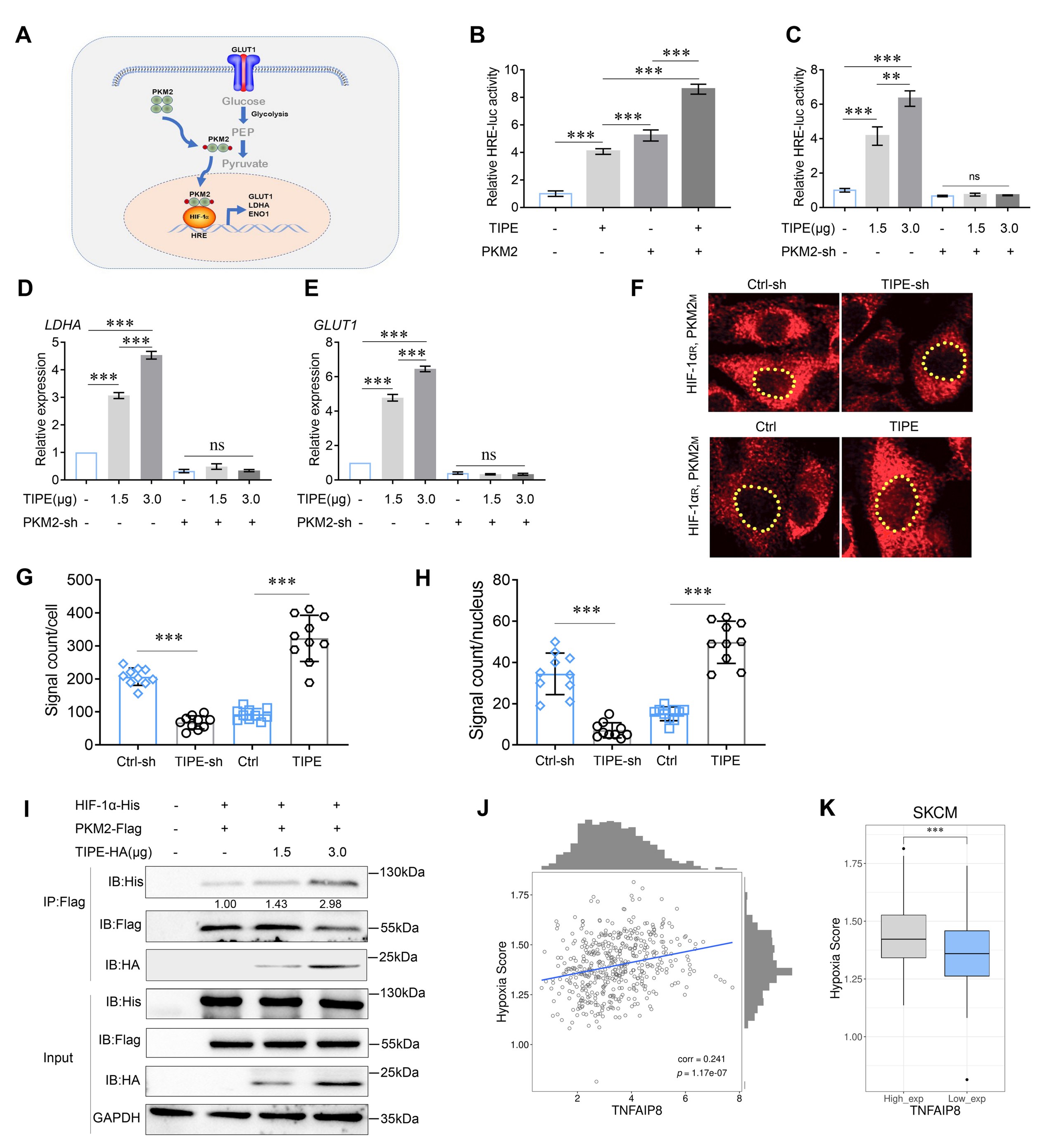
A
GLUT1
PKM2
Glucose
Glycolysis
PEP
PKM2
Pyruvate
PKM2
HIF-1α
HRE
GLUT1
LDHA
ENO1
B
Relative HRE-luc activity
TIPE - + - +
PKM2 - - + +
C
Relative HRE-luc activity
TIPE(μg) - 1.5 3.0 - 1.5 3.0
PKM2-sh - - - + + +
ns
D
LDHA
Relative expression
TIPE(μg) - 1.5 3.0 - 1.5 3.0
PKM2-sh - - - + + +
ns
E
GLUT1
Relative expression
TIPE(μg) - 1.5 3.0 - 1.5 3.0
PKM2-sh - - - + + +
ns
F
Ctrl-sh
TIPE-sh
HIF-1αR, PKM2M
Ctrl
TIPE
HIF-1αR, PKM2M
G
Signal count/cell
Ctrl-sh
TIPE-sh
Ctrl
TIPE
H
Signal count/nucleus
Ctrl-sh
TIPE-sh
Ctrl
TIPE
I
HIF-1α-His - + + +
PKM2-Flag - + + +
TIPE-HA(μg) - - 1.5 3.0
IP:Flag
IB:His
130kDa
1.00 1.43 2.98
IB:Flag
55kDa
IB:HA
25kDa
Input
IB:His
130kDa
IB:Flag
55kDa
IB:HA
25kDa
GAPDH
35kDa
J
Hypoxia Score
TNFAIP8
corr = 0.241
p = 1.17e-07
K
SKCM
Hypoxia Score
High_exp
Low_exp
TNFAIP8

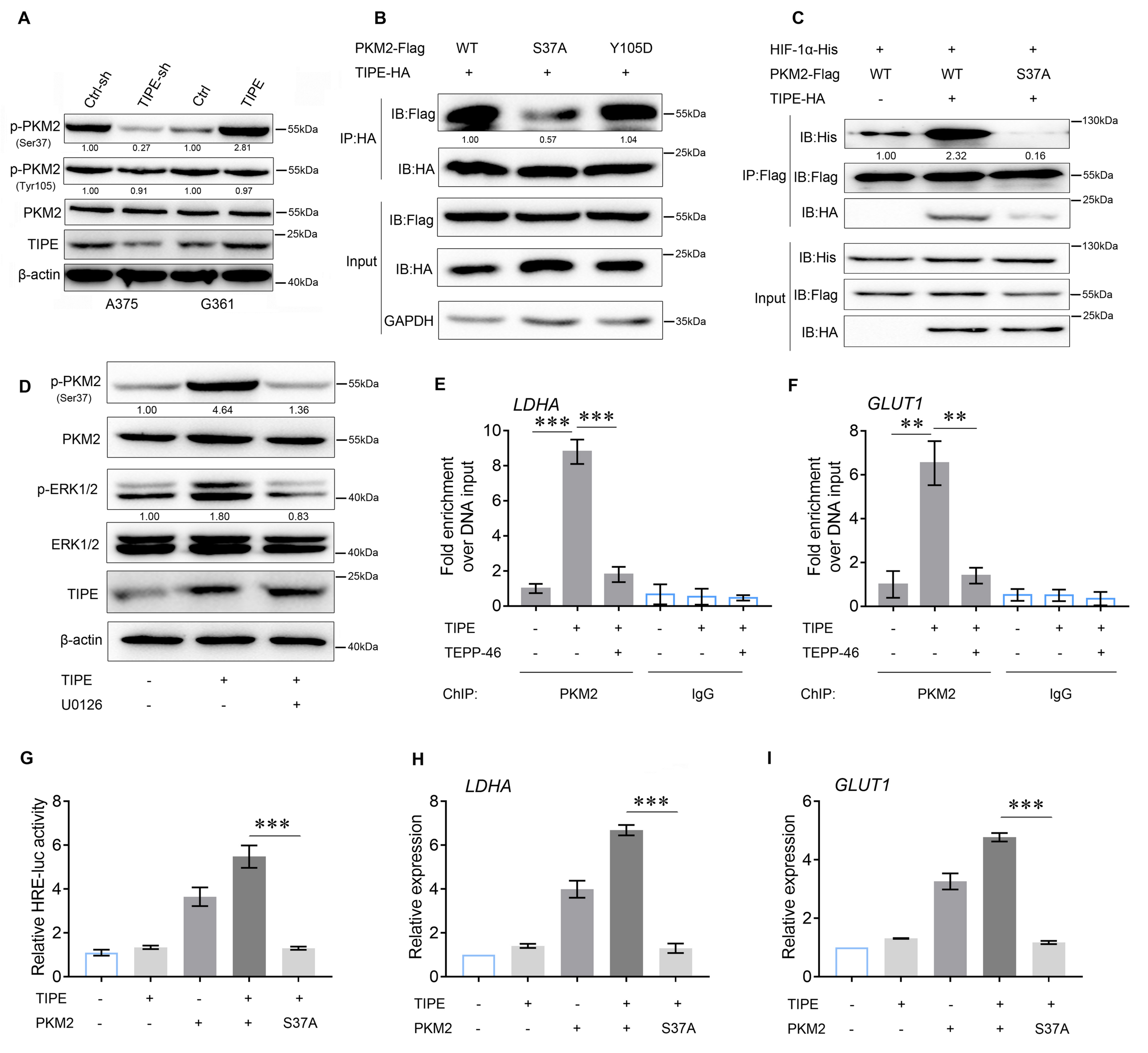
A
Ctrl-sh
TIPE-sh
Ctrl
TIPE
p-PKM2 (Ser37)
1.00 0.27 1.00 2.81
p-PKM2 (Tyr105)
1.00 0.91 1.00 0.97
PKM2
TIPE
β-actin
55kDa
25kDa
40kDa
A375
G361
B
PKM2-Flag WT S37A Y105D
TIPE-HA + + +
IP:HA
IB:Flag
1.00 0.57 1.04
IB:HA
Input
IB:Flag
IB:HA
GAPDH
55kDa
25kDa
35kDa
C
HIF-1α-His + + +
PKM2-Flag WT WT S37A
TIPE-HA - + +
IP:Flag
IB:His
1.00 2.32 0.16
IB:Flag
IB:HA
Input
IB:His
IB:Flag
IB:HA
130kDa
55kDa
25kDa
D
p-PKM2 (Ser37)
1.00 4.64 1.36
PKM2
p-ERK1/2
1.00 1.80 0.83
ERK1/2
TIPE
β-actin
55kDa
40kDa
25kDa
TIPE - + +
U0126 - - +
E
LDHA
Fold enrichment over DNA input
***
***
TIPE - + + - + +
TEPP-46 - - + - - +
ChIP: PKM2 IgG
F
GLUT1
Fold enrichment over DNA input
**
**
TIPE - + + - + +
TEPP-46 - - + - - +
ChIP: PKM2 IgG
G
Relative HRE-luc activity
***
TIPE - + - + +
PKM2 - - + + S37A
H
LDHA
Relative expression
***
TIPE - + - + +
PKM2 - - + + S37A
I
GLUT1
Relative expression
***
TIPE - + - + +
PKM2 - - + + S37A

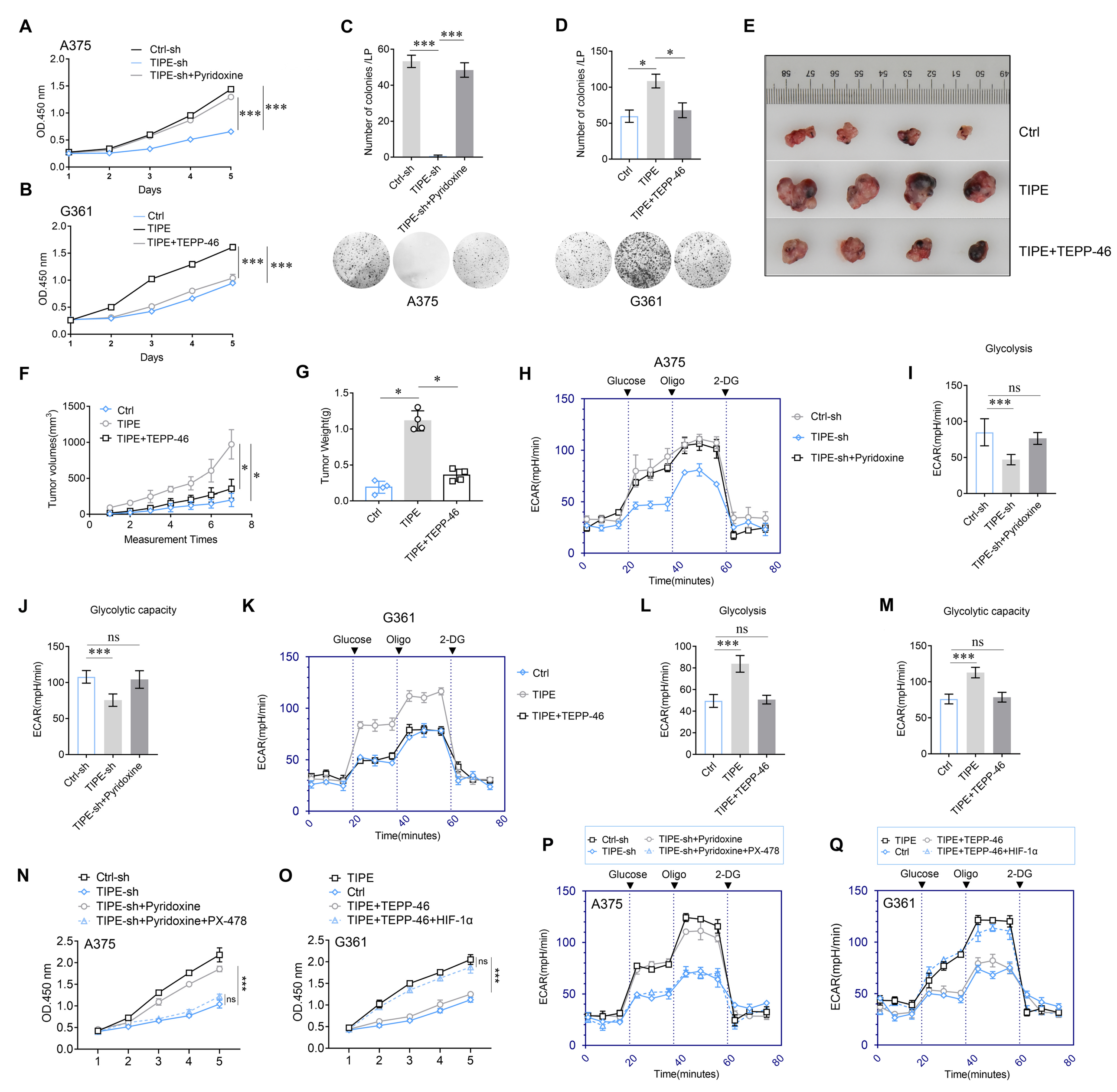
A
A375
Ctrl-sh
TIPE-sh
TIPE-sh+Pyridoxine
OD.450 nm
Days
B
G361
Ctrl
TIPE
TIPE+TEPP-46
C
Number of colonies /LP
Ctrl-sh
TIPE-sh
TIPE-sh+Pyridoxine
A375
D
Number of colonies /LP
Ctrl
TIPE
TIPE+TEPP-46
G361
E
Ctrl
TIPE
TIPE+TEPP-46
F
Tumor volumes(mm3)
Measurement Times
G
Tumor Weight(g)
H
A375
Glucose
Oligo
2-DG
ECAR(mpH/min)
Time(minutes)
I
Glycolysis
ECAR(mpH/min)
J
Glycolytic capacity
K
G361
L
Glycolysis
M
Glycolytic capacity
N
Ctrl-sh
TIPE-sh
TIPE-sh+Pyridoxine
TIPE-sh+Pyridoxine+PX-478
A375
O
TIPE
Ctrl
TIPE+TEPP-46
TIPE+TEPP-46+HIF-1α
G361
P
A375
Q
G361

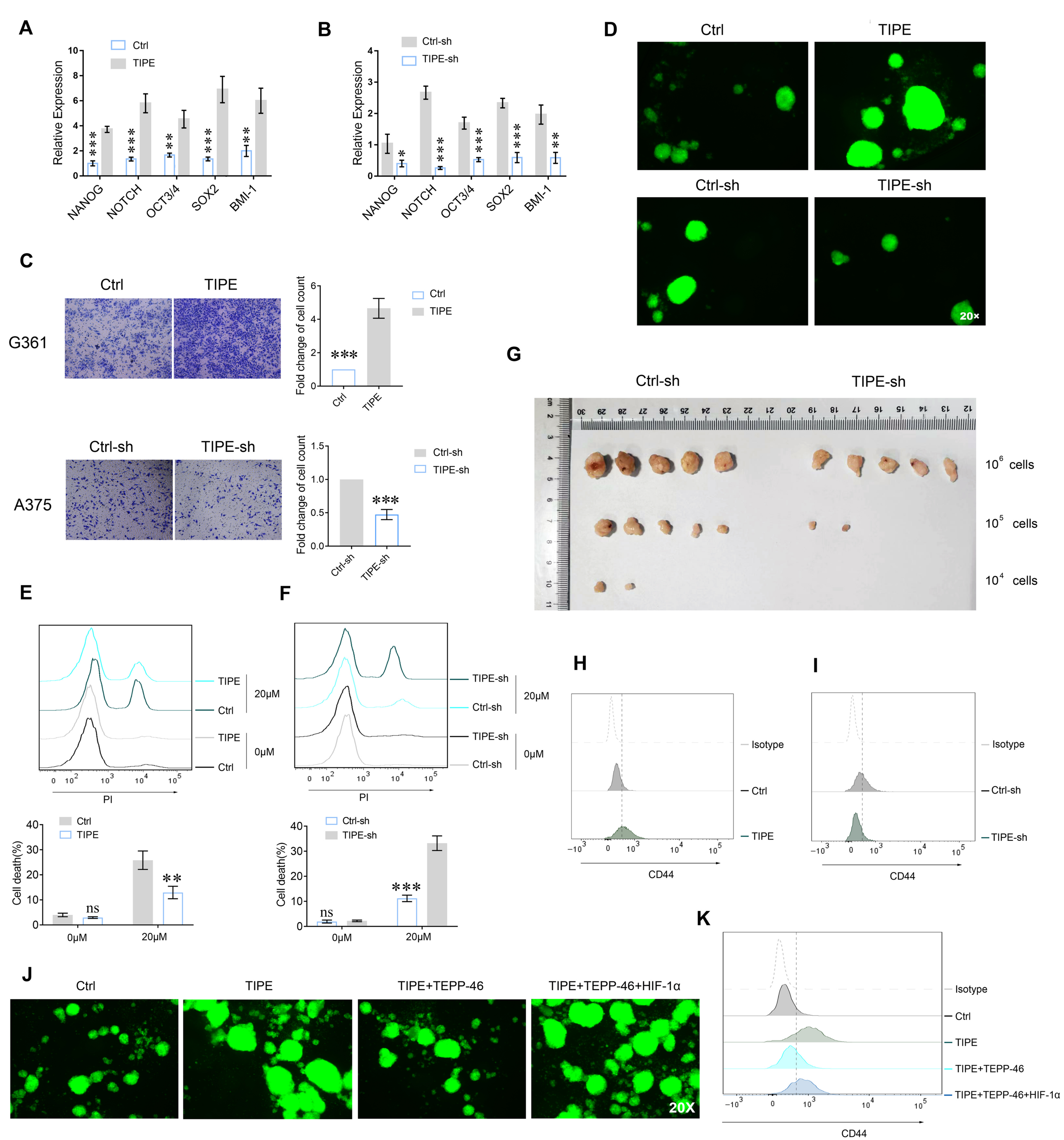
A
Ctrl
TIPE
Relative Expression
NANOG
NOTCH
OCT3/4
SOX2
BMI-1
B
Ctrl-sh
TIPE-sh
Relative Expression
C
Ctrl
TIPE
G361
Fold change of cell count
Ctrl-sh
TIPE-sh
A375
D
Ctrl
TIPE
Ctrl-sh
TIPE-sh
20×
G
Ctrl-sh
TIPE-sh
10^6 cells
10^5 cells
10^4 cells
E
TIPE
Ctrl
20μM
0μM
PI
Cell death(%)
ns
0μM
20μM
F
TIPE-sh
Ctrl-sh
20μM
0μM
PI
Cell death(%)
ns
0μM
20μM
H
Isotype
Ctrl
TIPE
CD44
I
Isotype
Ctrl-sh
TIPE-sh
CD44
J
Ctrl
TIPE
TIPE+TEPP-46
TIPE+TEPP-46+HIF-1α
20X
K
Isotype
Ctrl
TIPE
TIPE+TEPP-46
TIPE+TEPP-46+HIF-1α
CD44

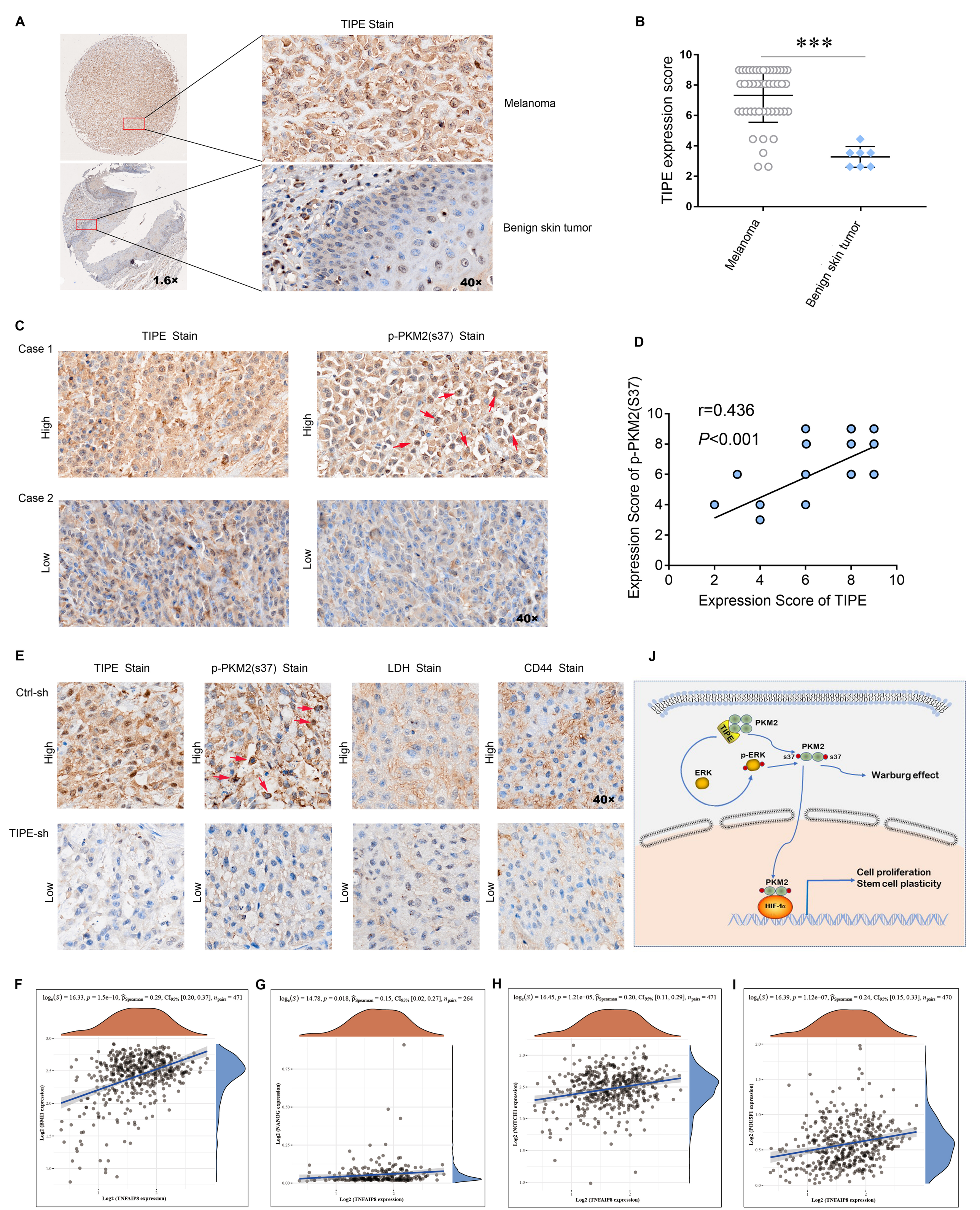
A
TIPE Stain
Melanoma
Benign skin tumor
1.6×
40×
B
***
TIPE expression score
Melanoma
Benign skin tumor
C
TIPE Stain
p-PKM2(s37) Stain
Case 1
Case 2
High
Low
40×
D
r=0.436
P<0.001
Expression Score of p-PKM2(S37)
Expression Score of TIPE
E
TIPE Stain
p-PKM2(s37) Stain
LDH Stain
CD44 Stain
Ctrl-sh
TIPE-sh
High
Low
40×
J
PKM2
TIPE
p-ERK
ERK
s37
Warburg effect
Cell proliferation
Stem cell plasticity
HIF-1α
F
G
H
I
Log2 (BMI1 expression)
Log2 (NANOG expression)
Log2 (NOTCH1 expression)
Log2 (POU5F1 expression)
Log2 (TNFAIP8 expression)